frontiers | Frontiers in Materials

TYPE Review
PUBLISHED 02 May 2023
DOI 10.3389/fmats.2023.1146045

Check for updates

OPEN ACCESS

EDITED BY
Enda McGlynn,
Dublin City University, Ireland

REVIEWED BY
Bowen Ji,
Northwestern Polytechnical University, China
Everson Thiago Santos Gerôncio,
Federal University of Piauí, Brazil
Yu-Qing Zheng,
Peking University, China
Jin Wu,
Sun Yat-sen University, China

*CORRESPONDENCE
Tzung K. Hsiai,
thsiai@mednet.ucla.edu

RECEIVED 16 January 2023
ACCEPTED 12 April 2023
PUBLISHED 02 May 2023

CITATION
Chen J, Arianpour B, Wang K, Wang S, Yin J, Zhang Y, Zhu E and Hsiai TK (2023), Emerging nanomaterials to enhance electrochemical impedance spectroscopy for biomedical applications.
Front. Mater. 10:1146045.
doi: 10.3389/fmats.2023.1146045

COPYRIGHT
© 2023 Chen, Arianpour, Wang, Wang, Yin, Zhang, Zhu and Hsiai. This is an open-access article distributed under the terms of the Creative Commons Attribution License (CC BY). The use, distribution or reproduction in other forums is permitted, provided the original author(s) and the copyright owner(s) are credited and that the original publication in this journal is cited, in accordance with accepted academic practice. No use, distribution or reproduction is permitted which does not comply with these terms.

Emerging nanomaterials to enhance electrochemical impedance spectroscopy for biomedical applications

Justin Chen[1], Brian Arianpour[1], Kaidong Wang[2], Shaolei Wang[1], Junyi Yin[1], Yaran Zhang[1], Enbo Zhu[2] and Tzung K. Hsiai[1,2]*

[1]Department of Bioengineering, University of California, Los Angeles, Los Angeles, CA, United States, [2]Division of Cardiology, Department of Medicine, David Geffen School of Medicine, University of California, Los Angeles, Los Angeles, CA, United States

Over the last few decades, electrical impedance-based sensors have been investigated for clinical translation to detect changes in tissue conductivities, including cardiac output and pulmonary function. Recently, electrochemical impedance spectroscopy (EIS) provides metabolic measurements that occur at the electrode-tissue interface, and the 3-D EIS can be reconstructed to generate electrical impedance tomography (EIT) for detecting the impedimetric properties of the vascular wall or fatty liver disease. In both EIS and EIT applications, the electrochemical properties of the interface electrodes are essential to address the signal-to-noise ratio or sensitivity of measurements in the biological environment. To enhance the conductive properties, we will survey a series of carbon-based nanomaterials as the emerging candidates for coating the electrodes of bioimpedance sensors. In this review, we will provide a theoretical background on impedance-based measurements and highlight the current state of EIS and EIT, including their applications for cancer screening and detection of vulnerable atherosclerotic plaques. Next, we will focus on the strengths of different nanomaterials when used as an electrode coating to optimize charge transfer across the electric double layers and to enhance measurement sensitivity. We will also identify some unmet clinical needs, such as the ability to adapt to different hemodynamic conditions and blood vessel geometries, that can be realized by the novel biomaterials for the future EIS-based sensors.

KEYWORDS

nanomaterials, electrochemical impedance spectroscopy, electrical impedance tomography, wearable devices, implantable materials

1 Introduction

Developing minimally invasive, clinically translational, and highly accurate sensors remains an unmet challenge in biomedical engineering (Henderson and Webster, 1978; Cho, 2008; Dean et al., 2008; Halter et al., 2008; Yu et al., 2011b; Zhang et al., 2018; Chakraborty et al., 2019; Choi et al., 2019; Tyler et al., 2020; Sella et al., 2021; Zhao S. R. et al., 2022). Currently, ultrasound and optical coherence tomography rely on the acoustic and optical properties of biological tissues, respectively, which are limited from detecting the metabolic states of tissues or organ systems (Yu et al., 2011b). To address this issue, investigators have sought to develop electrochemical impedance spectroscopy (EIS) as

a minimally invasive diagnostic method. EIS analyzes the impedimetric properties of a target tissue upon application of a low-amplitude (typically ≤ 10 mV) AC signal at the frequency sweep from 10 kHz to 300 kHz for vascular EIS measurement of lipid-laden plaques, and 50 kHz–250 kHz for liver EIT of fatty infiltrate, respectively (Cho, 2008; Merrill, 2010; Luo et al., 2018; Zhang et al., 2018; Chakraborty et al., 2019; Chang et al., 2021; Magar et al., 2021). The measured frequency-dependent impedance is fitted to an equivalent circuit consisting of resistors and capacitive elements to analyze mass-transfer, charge-transfer, and diffusion interactions that occur at the electrode-tissue interface. The frequency-dependent changes in EIS can be used to distinguish between tissue conductivities, from the least conductive bone to the conductive lipid (fatty)-enriched liver; thereby, predicting metabolically active arterial atherosclerotic plaques or fatty infiltrate in the liver.

Current biomedical applications of EIS principles span from molecular detection to organ imaging, and to intravascular sensing (Süselbeck et al., 2005; Lymperopoulos et al., 2017; Halter et al., 2008; Yu et al., 2011a; Yu et al., 2011b). Over the last decades, the number of electrodes on EIS sensors have been optimized for tissue-specific applications. While initial studies, such as that previously reported by Süselbeck et al. (2005), relied on four-point microelectrodes to detect the presence of neointimal proliferation on stented arteries, later studies implemented two-point electrodes allowing for integration with the catheter-based imaging modalities, such as intravascular ultrasound (IVUS) (Cao et al., 2014; Packard et al., 2016). In addition to reducing the dimension of the system, the two-point electrode systems for EIS measurement are capable of common mode rejection of alternating current (AC); thus, allowing for deep arterial wall penetration in the space-confining environments and a higher signal-to-noise ratio (SNR) (Packard et al., 2016). These advantages of two-point EIS reside in the feasibility for integrating multiple pairs of EIS electrodes for 3-D reconstruction of electrical impedance tomography (EIT) for endoluminal detection of lipid-laden plaques (Abiri et al., 2022). Abiri et al. (2022) further demonstrated that increasing the number of microelectrodes of an EIS system improves the spatial resolution for the EIT measurement. By implementing a 6-point system for interrogation of the carotid arteries of a Yucatan mini-pig model of atherosclerosis, fifteen permutations of intravascular measurements were able to be recorded within the frequency range from 1 kHz to 300 kHz, resulting in high-resolution EIT reconstructions for endoluminal mapping of the lipid-laden plaques (Henderson and Webster, 1978; Mansouri et al., 2021; Abiri et al., 2022).

However, designing microelectrodes to optimize the impedance measurement remains a challenge for intravascular interrogations. One way of overcoming this obstacle is to reduce the impedance of the electrochemical double layer between the electrodes and tissue surface, as illustrated by Eq. **1**, where Z denotes the electrical impedance, R the real resistance, j the imaginary operator ($j \equiv \sqrt{-1}$), and X_c the reactance (Yu et al., 2011a; Packard et al., 2017; Abiri et al., 2022).

$$Z = R + jX_c \tag{1}$$

The resistive component R could further be expressed as $\rho\ell/A$, where ρ denotes resistivity, ℓ the length, and A area, demonstrating that the impedance is inversely dependent on the surface area of the electrodes. However, space-limiting intravascular applications is not conducive to increasing the surface area (Hinderliter et al., 2006). Alternatively, electrode coatings have been applied to increase the surface roughness (Packard et al., 2017). Materials, which increases the effective surface area, typically exist at a nanoscopic level (Hu et al., 2008). In this context, this review will introduce nanomaterials aligning with the safety parameters and biocompatibility to mitigate immune reaction and blood coagulation for the Federal Drug Administration (FDA) approved biomedical applications (Suni, 2008; Hondroulis et al., 2012; Cao et al., 2014; Shah et al., 2015). Furthermore, biomedical applications of EIS or EIT will consider the specific absorption rate (SAR), which defines the level of energy absorbed by the body per unit time, and the FDA limits the average SAR to 4 W/kg over the course of 15 min (Seo and Wang, 2021). Given these constraints, we will highlight the emerging nanomaterials to enhance the sensitivity of EIS or EIT measurements.

2 Background of electrochemical double layer for impedance measurements

EIS is defined by fitting the bioimpedimetric data to equivalent circuits, and a well-accepted model is the Randles circuit (**Figure 1A**) (Merrill, 2010; Magar et al., 2021; Jash et al., 2022). This equivalent circuit consists of two domains. The first domain is the series resistance R_s, which represents the linear impedances of the biological tissue, and the second domain is a three-element mesh that models the non-linear ionic interactions occurring at the electrode-tissue interface (Magar et al., 2021). The mesh consists of a constant phase element (CPE), a Warburg diffusion element (W), and a charge transfer resistance (R_{ct}). The CPE serves as a non-Faradaic pseudocapacitor with an impedance function described by Eq. **2** (Franks et al., 2005; Packard et al., 2017; Holm et al., 2021; Magar et al., 2021). Its corresponding capacitance can be simplified as C_{dl}, where Y_0 is the admittance parameter, and α is a fractional constant that describes the relative behavior of the element.

$$Z_{CPE} = \frac{1}{Y_0(j\omega)^{\alpha}}, \quad 0 \le \alpha \le 1 \tag{2}$$

A value of $\alpha = 1$ denotes an ideal capacitor with capacitance Y_0, while a value of $\alpha = 0$ denotes an ideal resistor with resistance $1/Y_0$ (Franks et al., 2005; Holm et al., 2021). The Warburg diffusion element is a specific case of the CPE where $\alpha = 0.5$. This impedance function can be derived from Fick's second law of diffusion, capturing the passive transport of ions through the electrochemical double-layer (Skale et al., 2007). Lastly, R_{ct} is a constant element that quantifies the baseline impedance associated with a Faradaic reaction (Merrill, 2010; Magar et al., 2021).

Taken together, the electrode-tissue interface is an electrochemical double layer (**Figure 1B**). The region immediately adjacent to the charged electrode surface is known as the Stern Layer (Davis et al., 1978; Brown et al., 2016; Lin et al., 2020). Here, oppositely-charged ions closely adhere to the electrode, forming a thin, immobile surface with high potential energy. Past this is the diffuse layer, which contains both positively- and negatively-charged molecules aggregated in a highly organized topological

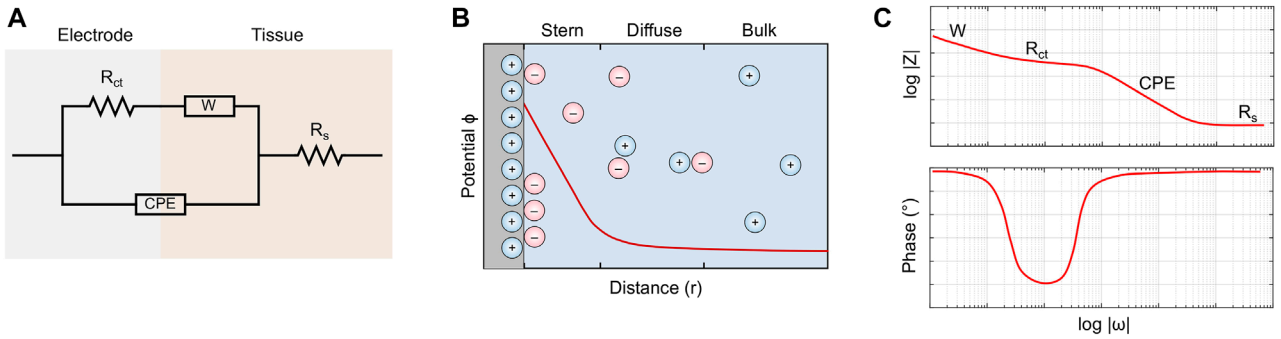

FIGURE 1
(A) The Randles equivalent circuit captures both Faradaic and non-Faradaic ionic interactions occurring at the electrode-tissue interface. **(B)** The interface is modeled as an electrochemical double layer. The Stern region consists of oppositely-charged ions that adhere to the electrode surface, while the diffuse layer consists of highly organized aggregates. **(C)** A bode plot showing the impedance of the equivalent circuit as a function of frequency. Impedances of high frequencies tend to the value of R_s.

configuration. Due to screening effects and cancellation of charges, the electric potential decays exponentially until steady state is achieved in the bulk tissue (Kesler et al., 2020).

Combining the circuit elements, we obtain a complete impedance function for the electrochemical system, as described by Eq. **3** (Bredar et al., 2020; Lai et al., 2020).

$$Z_{tot} = \frac{Z_{dl}(Z_{ct} + Z_W)}{Z_{dl} + Z_{ct} + Z_W} + Z_s \approx \frac{R_{ct}}{1 + R_{ct}C_{dl}(j\omega)} + R_s \qquad (3)$$

In principle, EIS characterizes tissues based on their impedimetric response across a range of frequencies (Magar et al., 2021). The values of the circuit elements are fitted from experimental results, which are either portrayed by a Bode plot or a Nyquist plot. A generic bode plot (**Figure 1C**) shows that the total impedance is undesirably high at low frequencies, which can be attributed to the diffusion of charge at the electrochemical double layer, as captured by the Warburg element. At high frequencies, the total impedance approaches the value of the tissue resistance R_s, effectively rendering the effects of the electrochemical double layer negligible (Carminati et al., 2022).

Compared with other biosensing modalities, the primary advantage of EIS is its ability to leverage multi-frequency analysis, making it desirable for tissue sensing applications (Magar et al., 2021). A set of frequencies is chosen to maximize the impedimetric difference between the target tissue and its environment. A computational algorithm can evaluate the EIS data at these frequencies to predict the type and severity of disease, as evidenced by a recent work performed by Banerjee et al. (2022), which successfully applied a machine learning model to characterize bone mineral content.

However, EIS is limited by the inability to distinguish between specific and non-specific binding for molecular sensing applications (Bogomolova et al., 2009). Other biosensing techniques, such as cyclic voltammetry (CV), square wave voltammetry (SWV), and quartz crystal microbalance (QCM), aim to address this issue by providing additional information about the target molecule (Lim et al., 2020; Liu et al., 2022). CV operates by applying a triangular scanning potential to the working electrode, which induces a series of oxidation and reduction reactions (Liu et al., 2022). SWV is another technique that is similar to CV, but the scanning potential is a staircase wave superimposed with a symmetrical square wave. For both applications, the corresponding peaks are visualized on a voltammogram, which shows the relationship between voltage and current. Though CV and SWV allow us to quantify important aspects of the reaction mechanism, such as rate and concentration, these methods can be influenced by the pH of the solution and other environmental factors. To this end, QCM has been developed as a method to distinguish molecules by molecular mass, yielding a sensitivity on the order of nanograms per cm^2 (Lim et al., 2020). A complete summary of the comparison between EIS, CV, SWV, and QCM can be found in **Table 1**.

Overall, the sensitivity of EIS can be enhanced through the implementation of highly conductive nanomaterial coatings to reduce the parasitic effects of the electrochemical double layer (Kesler et al., 2020). Examples of such nanomaterials will be further discussed in the following section.

3 Nanomaterial coatings for EIS sensors

Emerging nanomaterials have been investigated as promising candidates for improving the detection performance of EIS sensors (Jash et al., 2022). For a nanomaterial to be clinically translational, it must minimize the impedance of the electrochemical double layer, while demonstrating biocompatibility. Biocompatibility is a broad term that describes the ability of the host immune system to accept foreign materials (Yoshioka et al., 2016). For *in vivo* EIS applications, such as intravascular devices, it is important to prevent activation of the complement system and coagulation cascade. The complement system consists of specialized proteins that bind to foreign substances to facilitate clearance by phagocytic cells, whereas the coagulation cascade consists of a series of factors that trigger the formation of blood clots as a means to prevent blood loss. For EIS devices that come in contact with the skin, it is important to avoid allergic reactions, such as inflammation induced by mast cells (Yoshioka et al., 2016; Ud-Din et al., 2020).

TABLE 1 Comparison of biosensing modalities.

	Principles	Advantages	Limitations
EIS	• Low amplitude AC is applied to biological tissue across a range of frequencies (Magar et al., 2021) • Impedimetric data is measured and used to determine the presence of certain cells or tissues	• Can leverage multi-frequency analysis to further distinguish between tissue types (Magar et al., 2021)	• Unable to distinguish between specific and non-specific binding in molecular applications (Bogomolova et al., 2009)
CV	• Triangular scanning potential is applied to the working electrode (Liu et al., 2022) • Electroactive biological species undergoes continuous oxidation and reduction reactions • Corresponding peaks are visualized on the voltammogram	• Able to quantify aspects of the reaction mechanism, such as its rate (Liu et al., 2022) • Provides information about the concentration of the target analyte	• Dependent on the pH value of solution (Fahmy Taha et al., 2020) • Electrochemical reactions may induce enzymatic instability
SWV	• Similar to CV, but the scanning potential is a staircase wave superimposed with a symmetrical square wave (Liu et al., 2022) • Current is measured at the end of each pulse to identify the biological target	• Able to quantify aspects of the reaction mechanism (Liu et al., 2022) • Faster detection speed with a shorter potential period • Ability to analyze reversible or quasi-reversible processes	• Yields a low response, especially when the electrode reaction occurs at a slow rate (Mirceski et al., 2018)
QCM	• Piezoelectric effect due to an external electric field causes oscillation in the thin disc of quartz (Lim et al., 2020) • Target molecule characterized by a mass variation through a mechanical transducer	• Can detect virtually all biological molecules since mass is an intrinsic property (Lim et al., 2020) • Sensitivity on the order of nanogram per cm^2	• Application is typically limited to molecular sensing (Lim et al., 2020)

Fortunately, many nanomaterials are able to be conjugated to functional groups so that their biocompatibility and conductivity can be optimized. Here, we examine the strengths and limitations of these nanomaterials-coated EIS electrodes. A summary of which is shown in **Table 2**.

3.1 Graphene and its derivatives

Reduced graphene oxides (rGOs) are a form of graphene that have been functionalized with oxygen-based groups, such as carbonyls or hydroxides, rendering more impedimetric stability for biological applications (Tarcan et al., 2020). One of the unique properties of rGOs is their ability to significantly reduce the impedance of the double layer in an electrochemical cell (Zhang et al., 2012; Xu et al., 2015). This reduction in impedance is due to the high surface area and excellent conductivity of rGOs, allowing for effective transfer of ions within the electrochemical double layer. In an atomic force microscopy (AFM) experiment, the average surface roughness of rGOs was measured to be 177 nm, which is much greater than that of traditional graphene (~ 47 nm) and gold nanostructures (< 5 nm) (Siegel et al., 2012; Zhang et al., 2012). Such a rough surface is conducive to the convective and diffusive transfer of charged particles. Moreover, rGO-based electrodes have the ability to harness π-stacking interactions that occur between the aromatic groups of the target tissue and the electrode surface, which further facilitates charge transfer for impedance reduction (Kim et al., 2013; Chen T. et al., 2018).

Over the last decade, graphene-based EIS sensors have garnered much attention due to their desirable impedimetric properties (Kim et al., 2013). One application of graphene is in the development of sensors to detect the water composition of human breath. Although graphene is hydrophobic in its original form, it can be conjugated to hydrophilic groups to increase water permeability and further increase its three-dimensional surface area (Lee et al., 2016). Using this technique, a composite lignosulfonate (LS)/rGO humidity sensor was reported to monitor breathing frequency by analyzing fluctuations of water molecules in human breath (**Figure 2A**) (Chen C. et al., 2018). The real-time sensing of breathing processes could be further exploited as an early warning system for sudden infant death syndrome and sleep apnea (**Figure 2B**) (Yang et al., 2019). Another application of graphene-derived nanomaterials is in the field of electroencephalography (EEG) sensors (Choi et al., 2019). In addition to the aforementioned properties, two-dimensional graphene films layered on parylene C substrates demonstrate high conformability on tissue-specific surfaces, resulting in low contact impedance and high SNR (Park et al., 2014). Accordingly, several studies have developed implantable graphene oxide (GO) microelectrode arrays for high-resolution neurophysiological recording and stimulation (Park et al., 2014; Lu et al., 2016; Xu B. et al., 2021). Overall, we observe the applications of graphene-derived nanomaterials in numerous wearable and implantable biomedical devices (**Figure 2C**), where their effectiveness in enhancing the sensitivity of EIS measurements can be attributed to the high surface roughness and unique electromechanical properties (Choi et al., 2019).

3.2 Metal-organic frameworks and their derivatives

Metal-organic frameworks (MOFs) are formed by metal ions and organic ligands via strong coordination bonds (Wang et al., 2018a; Wang et al., 2018b; Wang et al., 2019; Wang et al., 2020). They

TABLE 2 Comparison of nanomaterials for the enhancement of EIS.

	Advantages	Applications	Average surface roughness
Graphene	• Tunable chemistry (Tarcan et al., 2020) • π-stacking interactions (Kim et al., 2013)	• Humidity sensors for monitoring of breathing frequency (Chen et al., 2018a) • EEG (Choi et al., 2019)	• 47 nm (Traditional Graphenes) (Zhang et al., 2012) (Chen et al., 2018a) • 177 nm (rGOs)
MOFs	• Tunable chemistry (Raptopoulou, 2021) • Diverse structures and high porosity (Wang et al., 2022c)	• Bacterial detection sensors (Wang et al., 2021b) • Drug detection (Su et al., 2017)	• 3.5 nm (TFA) (Wang et al., 2022c) • 19 nm (UiO-66-4F) • 34 nm (UiO-UiO-66-NH_2)
Gold	• Biocompatibility (Ostovari et al., 2018) • Viable microenvironments (Huang et al., 2022)	• Immunosensors to detect harmful pathogens (Wen et al., 2017)	• Varies between 1.1 nm and 4.0 nm (Siegel et al., 2012)
Polymers	• Supramolecular π-π, van der Waals, and dipolar interactions to promote charge transfer (Nezakati et al., 2018; Yuk et al., 2020) • High conformability (Pan et al., 2020)	• Skin-compliant ionic sensors (Pan et al., 2020) • Biomimetic skin (Park et al., 2022)	• 1.5 nm (Gasiorowski et al., 2013)
MXenes	• Active sites (Iravani and Varma, 2022) • Porous structures (Castro et al., 2022)	• Theranostic sensor to detect muscle fatigue (Song et al., 2022) • Immunosensor for the detection of SARS-CoV-2 (Castro et al., 2022)	• 12 nm for single-layer coatings (Zukiene et al., 2021)
MoS_2	• Flexibility and ability to self-assemble (Yuan et al., 2015; Yan et al., 2022) • Weak van der Waals interaction to reduce strain (Yan et al., 2022)	• Detection of toxic gasses (Moore et al., 2022) • Sweat sensors (Pang et al., 2020)	• 0.33 nm (Yuan et al., 2015)

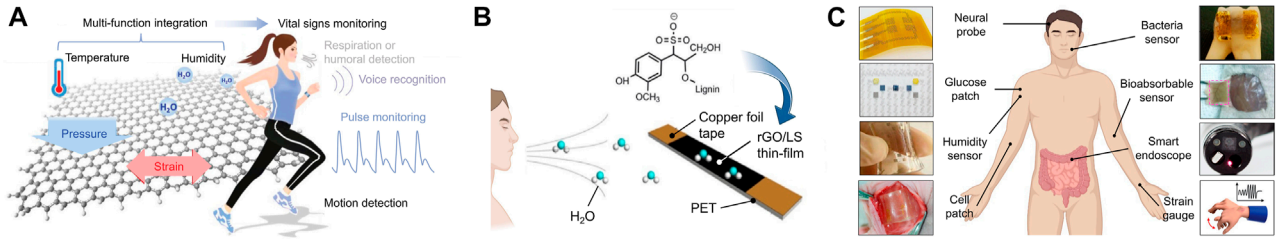

FIGURE 2
(A) Brief overview of a flexible graphene-based sensor platform. **(B)** A humidity sensor was fabricated based on an (LS)/rGO composite thin-film. **(C)** Wearable and implantable soft bioelectronics using 2D materials. [adapted and modified from (Choi et al., 2019; Yang et al., 2019)].

serve as promising candidates for the coatings of electrochemical sensors because of their diverse structures and large effective surface areas (**Figure 3A**) (Qiu et al., 2019). Similar to graphene, the surfaces of MOFs can be functionalized with a variety of organic ligands so that they can be tuned for specific applications (Raptopoulou, 2021). AFM results from a previous study concluded that the impedimetric properties of MOFs varies based on the particular ligand used for synthesis (Wang Y.-M. et al., 2022). For instance, the average surface roughness of TFA was measured to be 3.5 nm, UiO-66-4F 19 nm, and UiO-66-NH_2 34 nm. In addition to their tunable properties, MOFs have porous structures, making them effective for the absorption of ions. However, one drawback of MOFs is that they are poor conductors of electricity. Fortunately, this can be overcome by high-temperature pyrolysis treatment, which heats the material under oxygen-deprived conditions. Accordingly, the heat-treated MOFs would possess enough capacitance to reduce the impedance of the electrochemical double layer.

MOFs have generally been the preferred nanomaterial for molecular detection sensors because of their ability to facilitate highly specific surface reactions (Koo et al., 2019). In a previous study, an impedance immunosensor based on Mn-MOF-74 was designed to detect the concentration of *Listeria monocytogenes* (*L. m*) suspended in water and milk (Wang S. et al., 2021). The

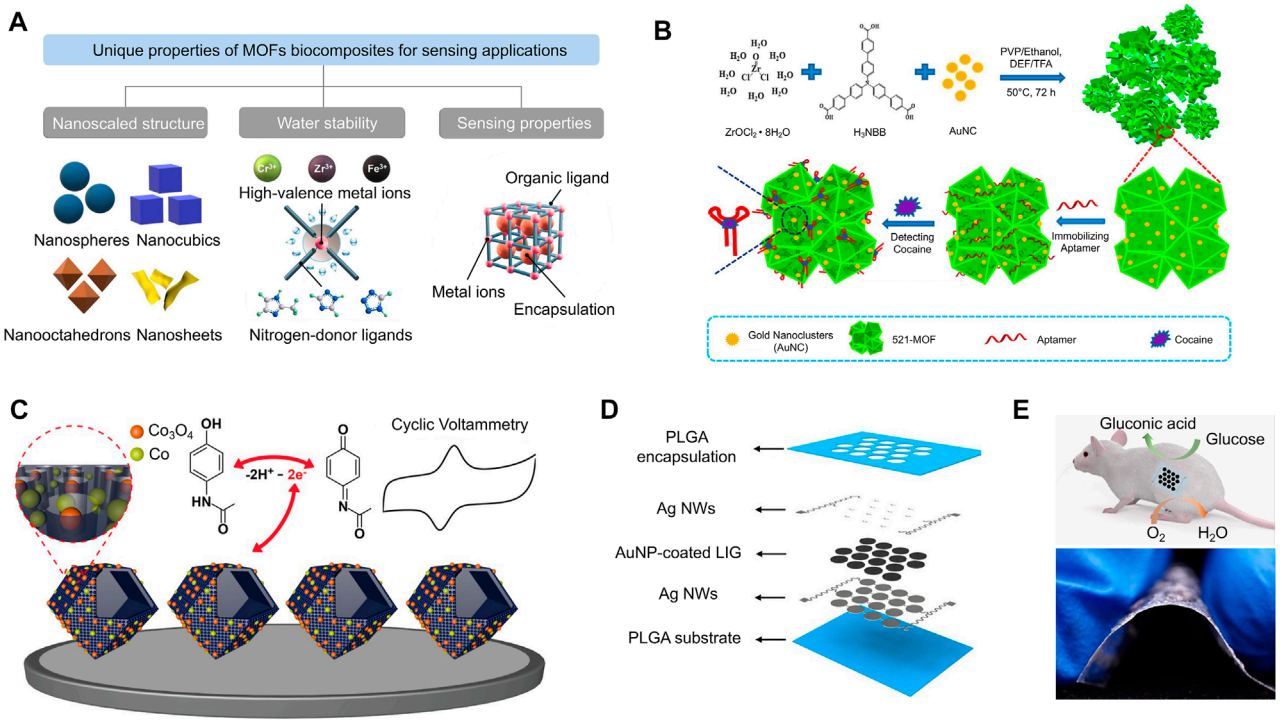

FIGURE 3
(A) MOFs have a variety of unique properties, such as nanoscaled structures and water stability, that make them useful for sensing applications. **(B)** A two-dimensional zirconium-based MOF (denoted 521-MOF) was conjugated to gold nanoclusters (AuNCs) in a one-pot reaction to serve as an aptamer-based biosensor for the detection of cocaine. **(C)** Co/Co_3O_4 nanoparticles are coupled with hollow nanoporous carbon polyhedrons for the enhanced electrochemical sensing of acetaminophen. **(D)** A graphic representation of a transient enzymatic biofuel cell array composed of LIG/Au nanoparticles, which is used as a nanogenerator for low-power implantable devices. **(E)** Implantation of the transient enzymatic biofuel cell array into a mouse model (top) and showing its flexibility (bottom). [adapted and modified from (Su et al., 2017; Qiu et al., 2019; Wang et al., 2019; Huang et al., 2022)].

addition of H_2O_2 causes the *L. m*-bound sensor to release Mn^{2+}, which is subsequently measured by frequency-dependent EIS. The molar concentration of Mn^{2+} should closely correspond to the original amount of *L. m* in solution, making Mn-MOF-74 an ideal nanomaterial for the ultra-sensitive detection of molecules. In another study, nucleic acid-MOF biocomposites were used to quantify the concentration of cocaine through its binding to a single stranded DNA (ssDNA) aptamer (**Figure 3B**) (Su et al., 2017; Qiu et al., 2019). 521-MOF was chosen for this application because it contains an abundance of Zr-O moieties, causing it to easily bind to the inorganic phosphates of ssDNA. However, this interaction is disturbed by the addition of cocaine because it blocks the transfer of electrons at the electrochemical double layer. To further enhance the sensitivity of the device, electrically conductive Au nanoclusters were deposited onto 521-MOF. Accordingly, the reported impedance sensor exhibited a low level of detection (LOD) of 0.44 pg mL^{-1}. To further expand the application of this device to detect other drugs, a different study developed a Co/Co_3O_4-based MOF to determine the presence of acetaminophen (**Figure 3C**) (Wang et al., 2019). Similar to graphene-based nanomaterials, MOFs increase the surface area and reduce the electrochemical double layer for developing sensitive biosensors.

3.3 Gold

Gold nanoparticles (AuNPs) are a well-established material for enhancing the performance of EIS sensors, where its primary advantage lies in its biocompatibility (Ostovari et al., 2018). Compared to conventional electrodes coatings, AuNPs provide a viable microenvironment for the detection of enzymes because they allow for more freedom in orientation (Huang et al., 2022). This makes them promising candidates for molecular and cellular detection devices. Moreover, AuNPs can be deposited into other substrates, such as laser-induced graphene (LIG) (**Figure 3D**), to further decrease electrical impedance for *in vivo* applications (**Figure 3E**) (Huang et al., 2022). This process causes rapid electron transfer between active sites and electrode surfaces, improving the performances of electrical outputs.

One previous study implemented a gold interdigitated array microelectrode into an immunosensor to detect harmful pathogens, such as *Salmonella Typhimurium*, contained in a 50 μL^{-1} solution (Wen et al., 2017; Strong et al., 2021). In addition to its biocompatibility, gold was chosen for this application because of its ability to conjugate to an *S. Typhimurium* antibody via streptavidin-biotin chemistry, further increasing the double layer capacitance for more precise measurements (Wen et al., 2017). Impedance signals

were acquired at a frequency range of 1 Hz to 1 MHz, where the most apparent impedance change between the bacteria and a negative control sample occurred at 101 Hz (Strong et al., 2021). At this frequency, the binding of *S. Typhimurium* to its antibody caused the impedance of the electrode-sample interface to increase from 15.08 to 20.45 kΩ, corresponding to a 36% difference from the control (Wen et al., 2017). Overall, the immunosensor exhibited high specificity and an average detection time of 1 h, suggesting the effectiveness of gold-coated electrodes for impedimetric reduction.

3.4 Conductive polymers

Conductive polymers are typically composed of an sp^2-hybridized backbone with alternating single and double bonds (Malhotra and Ali, 2018). This type of structure facilitates supramolecular π-π, van der Waals, and dipolar interactions to modulate covalent bonds for charge transfer (Nezakati et al., 2018; Yuk et al., 2020). One of the most widely used conductive polymers for electrode coatings is poly(3,4-ethylene dioxythiophene) polystyrene sulfonate (PEDOT:PSS) (Dijk et al., 2020). Due to its charged monomeric units, PEDOT:PSS promotes the Faradaic transfer of ions at the electrochemical interface, reducing the impedance by as much as a factor of 40, compared to conventional electrodes (Wang A. et al., 2021). Another conductive polymer for EIS applications is alginate-polyacrylamide (Alg-PAAm), which is a hydrogel-like material that demonstrates high conformability, similar to that of the thin graphene films previously discussed (Park et al., 2014; Pan et al., 2020). In addition, Alg-PAAm tends to form hydrogen bonds with macromolecules contained in human tissue, providing it with a unique adhesive property that aids in the minimization of parasitic impedance.

Detection instruments which integrate electronic circuits with gel ionic conductors display an excellent stretchability and sensing performance (Yao et al., 2022). For example, a skin-compliant ionic sensor coated with Alg-PAAm was reported to record electromyography (EMG) signals with an ultralow impedance of ~20 kΩ (**Figure 4A**) (Pan et al., 2020). The Alg-PAAm hydrogel shortened the electron transfer distance on the impedance sensor due to firm electrostatic interaction and multiple hydrogen bonds formations. Another application of gel ionic conductors involved the development of a biomimetic skin using multilayer hydrogel-silicone elastic composites prepared for tactile perception on robotic skin (Park et al., 2022). The electrical impedance signals were collected and processed by a deep convolutional neural network (Luo et al., 2018; Ravagli et al., 2020; Chang et al., 2021; Park et al., 2022). By taking advantage of the conformational properties of conductive polymers, ionic transport across the electrodes becomes more efficient, thereby producing more accurate EIT reconstructions.

3.5 MXenes

MXenes are a relatively new family of two-dimensional crystals, composed of transition metal carbides and nitrides (Naguib et al., 2011; Hantanasirisakul and Gogotsi, 2018). The main advantage of MXenes is the number of active sites, which enhance their catalytic abilities and selectivity for biosensing applications (Iravani and Varma, 2022). Accordingly, MXenes are able to detect biomarkers at low concentrations with a high accuracy rate. Other properties of MXenes that make it more advantageous to other nanomaterials are its excellent breathability, low sensor-skin interfacial impedance, and stable conductivity when exposed to sweat, as shown in **Figure 4B** (Song et al., 2022).

MXenes were used to fabricate a "theranostic" sensor to detect muscle fatigue and provide treatment (**Figure 4C**) (Song et al., 2022). Similar to MOFs, MXene-based electrodes have a porous structure, allowing them to store additional charge from surrounding electrolytes (Wang Y.-M. et al., 2022; Song et al., 2022). Accordingly, they maintain high conductivity while reducing irritation, making them a favorable candidate for electrothermal muscle fatigue treatment (Song et al., 2022). Another previous application of MXenes was in an immunosensor created for the early detection of severe acute respiratory syndrome coronavirus 2 (SARS-CoV-2) (Castro et al., 2022). This rapid and accurate COVID-19 screening technique is based on the interactions of the receptor-targeted binding. In particular, the device (**Figure 4D**) was coated with a peptide that mimicked the N-terminal domain (NTD) to recognize the anti-SARS-CoV-2 spike protein antibody. The charge transfer resistance was fitted from the impedance signals measured from a reversible redox probe in solution (Bolotsky et al., 2019). Compared to traditional uncoated electrodes, it was shown that the impedance signals of MXene possess "unique spikes" with lower amplitude, thereby improving the sensitivity of diagnostic sensors.

3.6 MoS_2

MoS_2 is another type of two-dimensional nanomaterial for EIS applications. Although its average surface roughness (~ 0.33 nm) is low compared to the materials previously discussed, the primary advantage of MoS_2 coatings is its flexibility and ability to self-assemble (Yuan et al., 2015; Yan et al., 2022). MoS_2 is characterized by weak van Der Waals interactions, which allow thin sheets to freely slide against each other, while maintaining structural integrity and reducing strain (Yan et al., 2022). Accordingly, MoS_2 is a promising nanomaterial for flexible electronics, energy converters, and skin-interfacing devices (Li et al., 2020).

2D MoS_2 nanomaterials have been used in electrical impedance sensors to demonstrate real-time impedance measuring for certain gasses (Moore et al., 2022). One study demonstrated how NO_2 can be detected by a 2D MoS_2 electrical impedance sensor at a concentration of 1 ppb, reporting an improvement of more than three orders of magnitude compared to a traditional device. Impedance changes are amplified when a target molecule binds to the MoS_2 semiconductor because of conformational changes. Using the same principle, another study reported a dynamic detection range from 1 to 500 ng mL^{-1} for the continuous detection of cortisol in human sweat as it binds to a MoS_2 nanosheet (Pang et al., 2020). Overall, the ability for MoS_2 devices to detect gaseous molecules with high sensitivities can be attributed to its high surface-area to volume ratio as well as its low dimensionality.

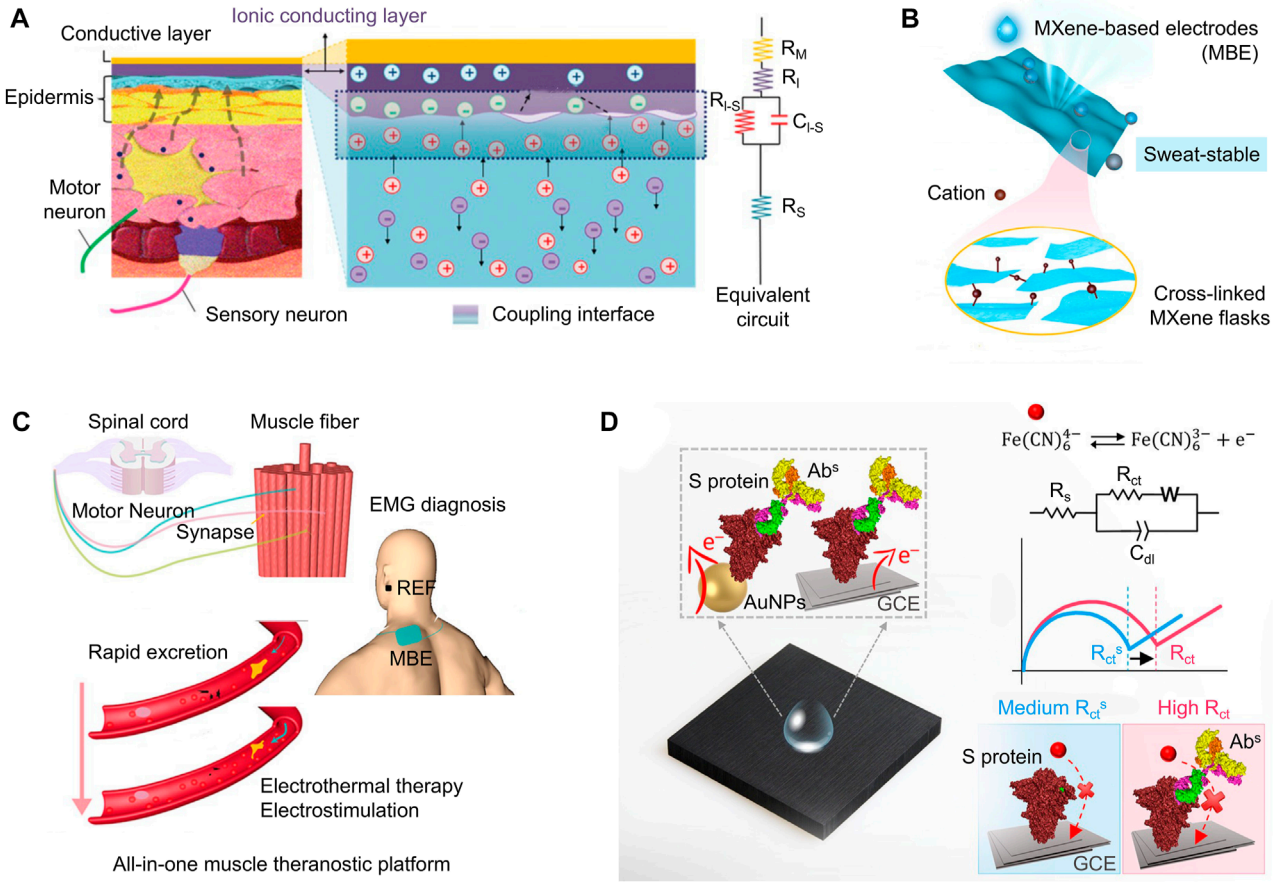

FIGURE 4
(A) A flexible skin-adherent electrode with minimal electrochemical impedance attached attached to the epidermis. An equivalent circuit model is shown to the right. **(B)** Bioderived, air-permeable, and sweat-stable MXene-based electrode (top), where structural crosslinking exists throughouth the nanoscopic structure (bottom). **(C)** A MXene-based "theranostic" device to provide electrothermal therapy if muscle fatigue is detected. **(D)** Loading a peptide onto a label free EIS biosensor increases its sensitivity. [adapted and modified from (Pan et al., 2020; Castro et al., 2022; Song et al., 2022)].

4 Applications of nanomaterials in wearable and implantable bioelectronics

In addition to EIS devices, emerging nanomaterials can be applied to the broader field of wearable and implantable bioelectronics. Here, we describe some of the recent advances in this field, focusing on how conductive nanomaterials are implemented to detect physiological signals with high SNR.

4.1 Wearable bioelectronics

Recently, wearable electronics for sweat analysis have attracted wide attention because they provide the detection of biomarkers, including electrolytes, metabolites, and proteins, which are related with body health status. The prerequisites for the sensing electrode contain decent mechanical deformability, high electrical conductivity, chemical inertness, and biocompatibility. To satisfy these properties, various materials and fabrication engineering strategies have been developed, including gallium-based liquids, conductive polymers, nanocomposites and strain engineering (Zhu et al., 2021; Ma et al., 2022; Li et al., 2022; Lv et al., 2021b; Lv et al., 2021a).

The nanomaterials of noble metals featuring high conductivity, excellent electrochemical stability, and large charge transfer capacity are emerging as novel sensing electrode materials for biomarker detecting devices, such as gold nanowires and nanosheets. For example, Cheng et al. reported vertically aligned mushroom-like gold nanowires (AuNW) serving as stretchable and wearable ion-to-electron transducers for multiplexed, *in situ* potentiometric sweat analysis (Zhai et al., 2020). The AuNW-embedded polydimethylsiloxane (PDMS) ensures the great intrinsic stretchability and mechanical duration of the sensor. As shown in **Figure 5A**, by attaching this wearable electrode on skin, the pH, Na^+, and K^+ can be non-invasively detected with high selectivity and stability even under 30% strain. Apart from AuNWs, porous Au coating is also utilized for the sensing electrode of sweat monitoring devices because of the highly improved effective surface area and electrical performance. As shown in **Figures 5A, B** wearable and disposable sweat-based glucose monitoring device with a feedback transdermal drug delivery module has been

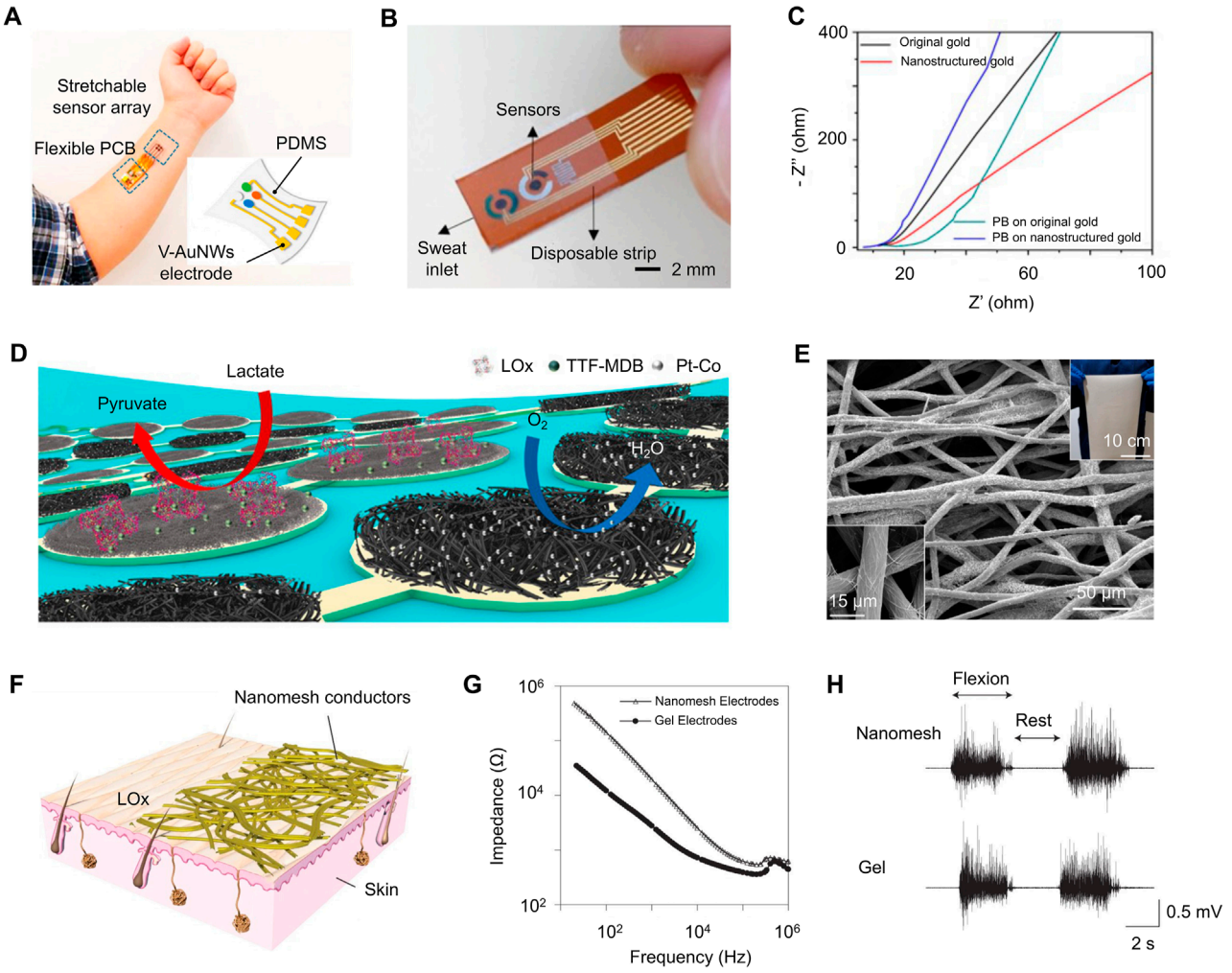

FIGURE 5
(A) An integrated wearable multiplexed sweat analysis device with AuNWs -based electrode array conforming on a subject's wrist. **(B)** Wearable/disposable sweat monitoring strip with porous Au coating. **(C)** Nyquist plot of EIS of O-Au (black), N-Au(red), O-PB (green), and N-PB (blue). **(D)** Schematic of a soft biofuel cells array consisting of LOx-modified bioanodes and Pt alloy nanoparticle–modified cathodes. **(E)** SEM image of AgNWs-coated conductive microtextile. Insets: A large microfiber textile (top-right) and a magnified SEM image. **(F)** A schematic of the Au-coated nanomesh conductors. **(G)** Impedance of the skin/electrode interface. **(H)** Electromyogram signals were measured on the forearm while the wrist was flexed at 90° (two times) and at rest by both nanomesh and gel electrodes. [adapted and modified from (Chen et al., 2017; Lee et al., 2017; Miyamoto et al., 2017; Yu et al., 2020; Zhai et al., 2020; Zhao et al., 2021)].

reported (Lee et al., 2017). A porous gold nanostructure was employed as the electrode to maximize the electrochemically active surface area for precise detection of glucose in sweat with high sensitivity. The nanostructured gold also provides a better deposition effect of other functional materials because of its larger surface area. Feng et al. reported an ultrathin (~3 μm) nanostructured biosensor for blood glucose monitoring (Chen et al., 2017). From the EIS analysis, the nanostructured gold electrode has lower diffusion resistance than the original gold electrode, as shown in Figure 5C.

Nanomaterials also played an important role in constructing self-powered wearable electronics. Power supply is also an important composition for next-generation wearable electronics (Xiao et al., 2022b). Apart from gold nanomaterials, carbon-based nanomaterials, such as carbon nanotubes (CNTs) and rGOs, have been widely investigated for self-powered wearable electronics because of their great conductivity, chemical stability and large surface area (Xiao et al., 2022a; Zhao X. et al., 2022; Mayer et al., 2022; Shen et al., 2022).

For example, Gao et al. reported a biofuel-powered soft electronic skin for key metabolic analytes (e.g., urea, NH_4^+, glucose, and pH) monitoring (Yu et al., 2020). They developed bioanode with rGO films with modified hierarchical Ni (h-Ni) microstructures, rGO films, and Meldola's blue–tetrathiafulvalene–modified carbon nanotubes (MDB-TTF-CNT) on an Au electrode. To form the BFC cathode, Pt-based nanoparticles were decorated on an MDB-modified CNT network (MDB-CNT) through electroless plating, as shown in Figure 5D. These nanostructured materials contribute to the high power intensity and long-term stability.

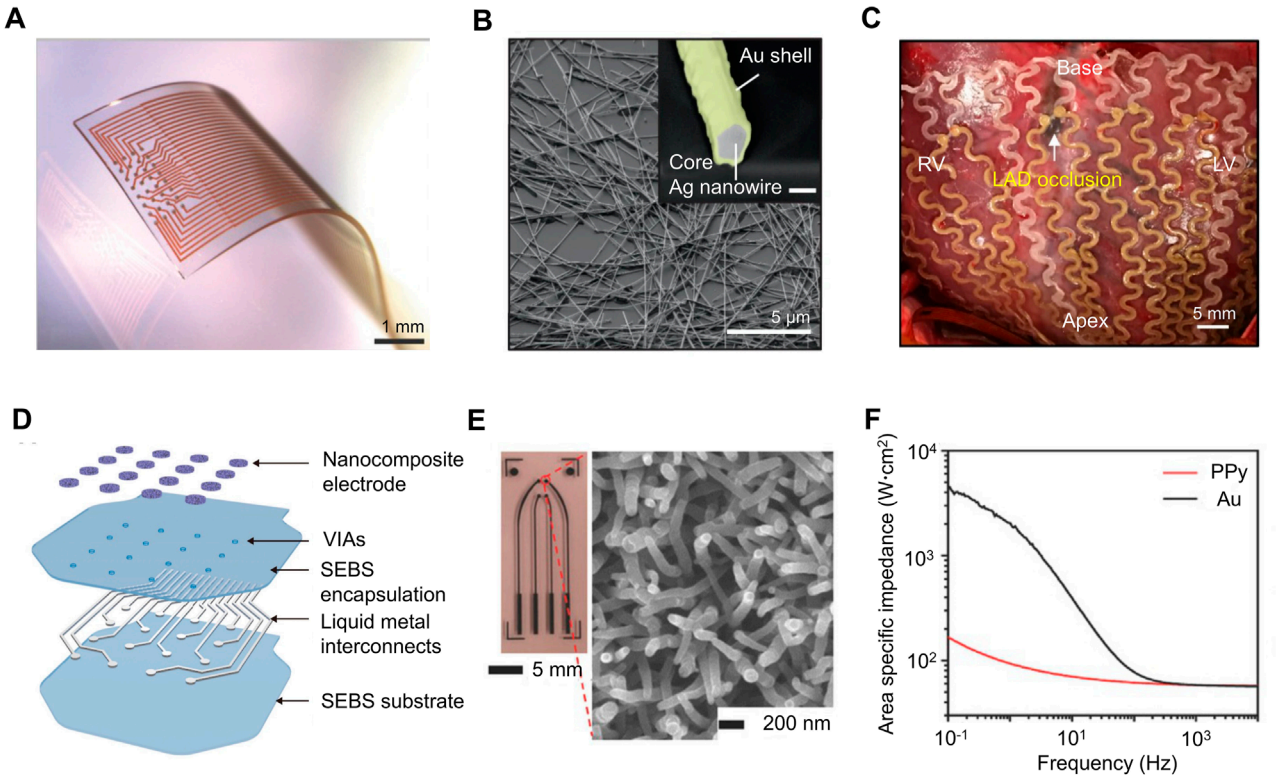

FIGURE 6
(A) Soft and stretchable electrode grids. The electrode grid is based on Au-TiO2NW conductors embedded in PDMS and comprises 32 electrodes with 200 μm pitch. Scale bars: 1 mm. **(B)** SEM image and backscattered electron (BSE) image (inset) of Ag-Au nanowires (before surface modification; Au sheath is in yellow). Scale bars, 5μm and 200 nm (inset). **(C)** Ag–Au nanocomposite-based implantable cardiac mesh for monitoring and stimulating swine heart *in vivo*. **(D)** Schematic showing the layer-by-layer construction of the liquid metal based electronic patch with nanocomposite electrodes. **(E)** Optical images of the multielectrode array (left) and SEM image of the PPy nanowires synthesized on the PPy electrode surface (right). **(F)** Electrochemical impedance spectra of the PPy film and Au film electrodes with the same geometric surface area. [adapted and modified from (Qi et al., 2017; Choi et al., 2018; Tybrandt et al., 2018; Wang S. et al., 2022)].

In recent years, integrating flexible conductors and electrodes with textiles to form the textile-based wearable devices has attracted much attention as their unique advantages include permeability, comfort, and aesthetic. In addition, coating nanomaterials on textiles with nanostructures also contributes to improving the electrical and mechanical performances of the sensing electrodes, such as large effective surface area, electrical conductivity, and stretchability. Kong et al. reported a conductive textile which is synthesized by bottom-up coassembly of silver nanowires and TPU microfibers, as shown in **Figure 5E** (Zhao et al., 2021). This conductive microtextile exhibits an excellent conductivity (>5000 S cm^{-1}), stretchability (~600% strain), soft mechanical properties, breathability, and washability. Because of its soft mechanical properties, the skin–electrode contact impedance of the conductive microtextile is marginally higher than state-of-the-art Ag/AgCl gel electrodes. Another article also proposed an ultrathin conductive nanomesh fabrication strategy (Miyamoto et al., 2017). In this report, they firstly deposited Au layers on PVA nanofibers to form a mesh-like sheet, then dissolved the PVA nanofiber with mater and finally got the highly gas-permeable, ultrathin and stretchable sensors, as shown in **Figure 5F**. The contact impedance with skin were comparable with gel electrodes and EMG signals were measured with the nanomesh electrodes, as shown in **Figures 5G, H**.

4.2 Implantable bioelectronics

In recent years, implantable electronics are emerging as the next-generation healthcare platforms for disease diagnosis and medical therapies. Conventional rigid electrodes tend to induce long-term inflammatory responses as the mechanical mismatch with soft biological tissues. Various nanomaterials such as nanostructured conductive polymers, metal-based nanowires and nanocomposite have shown great potential for the sensing electrode materials as their excellent electrochemical properties, soft mechanical performance and great biocompatibility. Vörös et al. proposed a design for neural interfacing microelectrode array based on an inert, high-performance composite material comprising gold-coated titanium dioxide nanowires embedded in a silicone matrix (as shown in **Figure 6A**) (Tybrandt et al., 2018). The platinum coating decreased the impedance of the electrodes by a factor of 5, with an areal capacitance of ≈ 2.7 mF cm^{-2}. For implantable electronics on the cardiac system, the mechanical deformation

property is an even more important consideration because of the constant heart beats. To solve the problem, researchers have proposed different strategies utilizing different nanocomposite as the sensing electrode. For example, Kim et al. reported a Ag-Au core–sheath nanowire composite (as shown in **Figure 6B**) and developed a soft and stretchable bioelectronic devices that can be conformally integrated with human skin and swine heart (**Figure 6C**) for continuous electrophysiological recording, and electrical and thermal stimulation (Choi et al., 2018). Another article proposed an innovative design for intrinsically stretchable electronics featuring the deployment of liquid metal components for ultrahigh stretchability up to 400% tensile strain and excellent durability against repetitive deformations, as shown in **Figure 6D** (Wang S. et al., 2022). By depositing a layer of micro-structured PEDOT:PSS on the Multi-walled Carbon Nanotube (MWCNT) nanocomposite, the interface impedance of the electrode is further reduced. In addition to metal nanowires, polymeric microelectrode array with nanostructured conductive polymers states for other biointegrated electronics. The compliant feature of conductive polymer enhances their compatibility with the soft biological tissues as well as impedance performance. As shown in **Figure 6E**, Chen et al. reported a polypyrrole (PPy) nanowire-based electrode for recording the electrocorticographic signals and stimulating the nerve of the rat (Qi et al., 2017). According to the EIS shown in **Figure 6F**, polymeric electrodes showed a much better impedance than those of the gold electrodes at lower frequencies (below 100 Hz) as their much larger surface area.

5 Biomedical applications of EIS

EIS sensors are currently being used for a variety of biomedical applications, in which biocompatibility, measurement accuracy, and device lifetime are important considerations when implementing novel nanomaterials (Magar et al., 2021). Here, we discuss the different biomedical uses of EIS sensors and the corresponding materials used for their fabrication processes.

5.1 Molecular detection

One of the biological applications for impedance-based sensors is molecular detection. In a pioneering study, a method was developed to detect the presence of protein with high specificity, in which a biotinylated aptamer was conjugated to a streptavidin-polymer-coated electrode made up of indium tin oxide (ITO) (Rodriguez et al., 2005). The biotinylated aptamer has a net negative charge, repelling the negative ions, $[Fe(CN)_6]^{3-/4-}$, from transferring electrons to the surface of the ITO electrode. Once selective binding of a specific protein to the aptamer occurs, the surface charge becomes an excess positive charge, which reduces the electron transfer resistance. This results in a highly specific and sensitive protein detection device that relies on electronic signals induced by protein-aptamer binding. Accordingly, the significance of this study is that it provides a label free EIS system that can be used for specific molecular detection.

Other choices for electrode materials include AuNPs and carbon-based nanomaterials. AuNPs have been previously designed to form nanoparticle-biomolecule conjugates inside a solution phase (Suni, 2008). The formation of such a complex amplifies the impedance signals, which effectively increases the signal-to-noise ratio. More recently, carbon-based nanomaterials have become a popular coating for molecular detection devices because of its ability to achieve a greater measurement specificity. For example, a composite electrode made of CNTs and PDMS were implemented into the original ITO protocol to aid in the specific detection of DNA (Moon et al., 2021). Compared to that of standard gold (Au) electrodes, the fabrication process of MWCNT/PDMS was more efficient, and therefore, more commercializable. Moreover, the composite coating was shown to have reduced the LOD from 25 p.m. to 20 fM for DNA.

After years of development, an ongoing challenge with impedance-based molecular detection sensors is integrating them into wearable devices. Recently, wearable technology has become a popular research topic due to their ability to provide personalized healthcare (Xu J. et al., 2021). Everyday clothing, such as shoes and watches, can serve as a means to deploy health-monitoring sensors. In one recent study, a non-invasive sweat sensor (**Figures 7A, B**) was created to monitor the concentrations of various nutrients and metabolites through electrochemical analysis (Wang M. et al., 2022). This sensor was designed to be a patch which has two graphene electrodes. These electrodes are repeatedly regenerated *in situ* with the integration of carbachol iontophoresis based sweat induction modules which assist with the microfluidic sweat sampling. The graphene electrodes are conjugated with synthetic antibodies and reporter nanoparticles to improve sensitivity and selectivity for a variety of biomarkers. With advances in the Internet of Things (IoT) technology, health data can easily be synchronized to the internet (**Figure 7C**) and interpreted by a physician in real time (Song et al., 2021). Another study conducted around the same time discovered that the serial impedance of the electrode slightly increases (<200 Ω) if the sweat sensor was stretched, although other parameters of the Randles circuit remain unchanged (Yin et al., 2022). Thus, a potential topic for future research is a correction algorithm that can normalize measurements taken from a stretched electrode.

5.2 Organ imaging

Another biological application of impedance-based sensors is the imaging of whole organs to diagnose abnormalities, such as tumors or diseased tissues, which could be performed with EIT (Henderson and Webster, 1978; Sella et al., 2021). During the initial stages of EIT, a major challenge was developing a signal-processing algorithm that can reconstruct the target organ. This issue was solved in the early 2000's with the creation of an open source MATLAB-integrated program called EIDORS, which still remains as the gold standard for EIT applications (Adler and Lionheart, 2006). The program consists of two parts: the forward problem and the inverse problem. The purpose of the forward problem is to describe the relationship between known parameters (i.e., the positions of the electrodes, conductivity, and current) and the resulting electrical potential distribution ϕ (Faia et al., 2012; Adler and Holder, 2022). Fundamentally, this procedure is described by Eq. **4**, which is derived from Maxwell's equations (Faia et al., 2012).

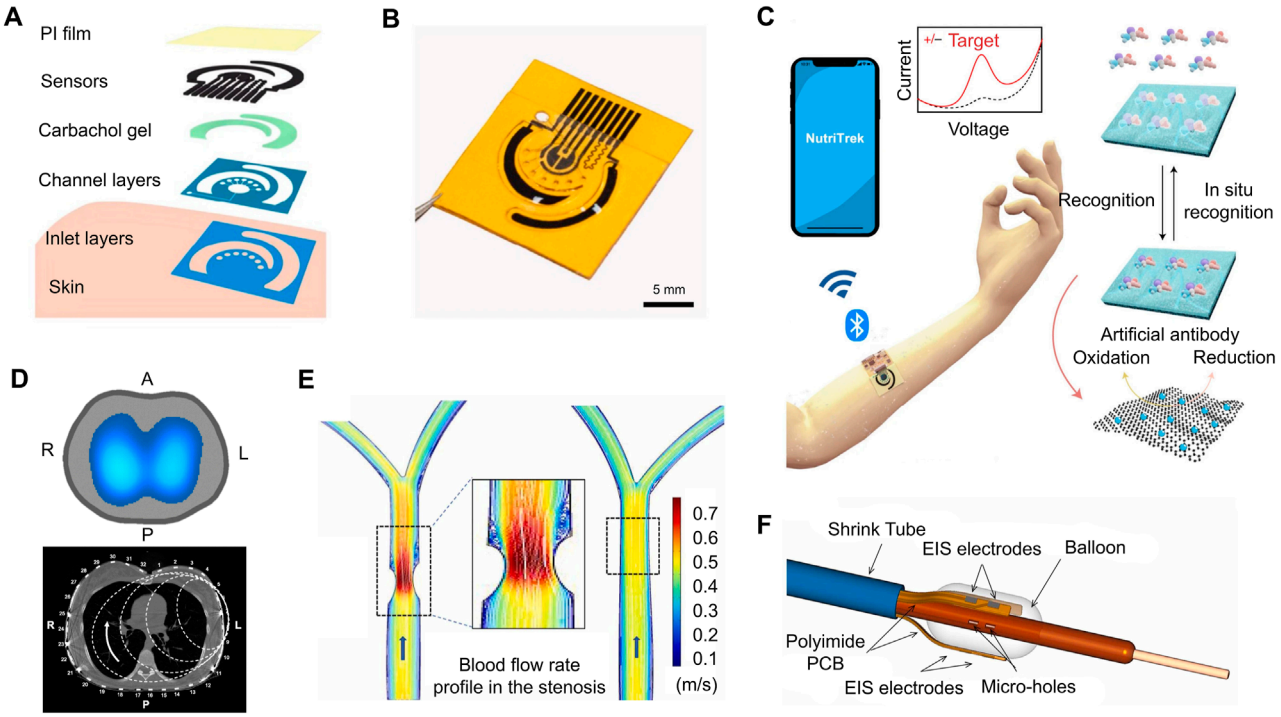

FIGURE 7
(A) A flexible patch for the detection of metabolites is comprised of a polyimide film, an electrochemical sensor, as well as several other layers to aid in signal conduction. **(B)** A three-dimensional rendering of the electrochemical sweat sensor. **(C)** IoT technology allows data from wearable electrochemical sensors to be synchronized to the cloud. Physicians could monitor such information in real time, further improving personalized healthcare. **(D)** An EIT belt is capable of diagnosing medical conditions by producing an impedance map of various organs, such as the lungs. **(E)** Blood flow restriction is present in the right carotid artery due to atherosclerosis. **(F)** EIS balloon catheter using six electrodes to develop 3-D images intravascularly. [adapted and modified from (Bachmann et al., 2018; Abiri et al., 2022; Wang M. et al., 2022)].

γ describes the complex admittivity, whose real and imaginary parts are dependent on the conductivity (σ) and permittivity (ε), respectively.

$$\nabla \cdot \gamma \nabla \phi = 0 \tag{4}$$

Once the forward problem is solved and the potential distribution is known, the next step is to reconstruct the conductivity distribution from measured electrical potentials at the boundary of the organ (Faia et al., 2012). This process is known as the inverse problem, and several mathematical methods have previously been proposed to solve for the reconstruction parameters. A well-accepted procedure is the Gauss-Newton algorithm, described in Eq. 5, where J is the Jacobian, ϕ the predicted potential from the forward problem, Φ the measured potential, α a regularization parameter, and R the regularization matrix.

$$\sigma_{i+1} = \sigma_i + \left(J_i^T J_i - \alpha R^T R\right) \cdot \left(J_i^T \left(\Phi_i - \phi\left(\sigma_i\right)\right) - \alpha R^T R \sigma_i\right) \tag{5}$$

The Gauss-Newton method is an iterative process that begins with an initial guess σ_0, which is unlikely to yield an accurate prediction (Adler and Holder, 2022). However, we can calculate an update, as given by the second term of Eq. 5, which is added to σ_0 to yield a more accurate estimate. This process is iterated until the final solution satisfies a pre-defined stopping criteria.

One clinical application of EIT is the diagnosis of pulmonary embolism, an arterial blockage in the lungs caused by blood clots (Lymperopoulos et al., 2017). The risk of pulmonary embolism is especially higher for patients who recently underwent surgery or had a certain illness, such as COVID-19 (Tapson, 2008; Sakr et al., 2020). Current method of diagnosis involves the insertion of radioactive materials into the lungs, which makes it easier to distinguish between regions of normal air flow and perfusion (Lymperopoulos et al., 2017). Since the use of x-rays and radioactive particles may be harmful to the patient, EIT offers a promising alternative to the diagnosis of pulmonary embolism. EIT devices are able to easily distinguish between blood, tissue, and air because of their distinct electrical conductivities. In recent years, several case reports have documented the successful application of EIT to identify pulmonary embolisms in post-operative patients (Wang X. et al., 2021; Kuk and Wright, 2022). Consequently, EIT data provided physicians with useful information, such as risk of bleeding, so they can make more informed decisions about prescription of anticoagulants and additional procedures. Another application of EIT is in the detection of non-alcoholic fatty liver disease (NAFLD), which is largely present in patients with obesity (Luo et al., 2018). In Western countries, NAFLD affects around 20%–50% of adults and is the most common liver disease in children (Brunt et al., 2015). Magnetic resonance imaging (MRI) is currently considered the gold standard for diagnosis of NAFLD, as it is non-invasive and highly accurate. However, some limitations associated with MRI are its high cost and its use of contrast agents. To overcome

these limitations, an EIT belt with 32 stainless steel electrodes was designed and tested on fat-fed New Zealand white rabbits and on human volunteers (Luo et al., 2018). It was shown that EIT measurements were most accurate at frequencies above 50 kHz, as validated by MRI data.

Recently, many EIT studies have shifted their focus towards improving the contrast ratio of the reconstructions so that diseased tissues can better be distinguished from healthy tissues (Brazey et al., 2022). To accomplish this, one study proposed the use of pure water, normal saline, and titanium dioxide (TiO_2) as sensitizers (Liu et al., 2013). The goal was to use these nanoparticles to enhance tissue impedance so that they can be more clearly measured by the transducer. Other studies have employed computational methods, such as Bayesian approximation, to enhance the contrast of EIT reconstruction (Nissinen et al., 2015).

Despite EIT technology having been around for several decades, its clinical usage still lags behind other imaging modalities (**Figure 7D**), such as computed tomography (CT) and magnetic resonance imaging (MRI) (Bachmann et al., 2018). Non-etheless, EIT remains a promising diagnostic tool, as its dependence on the electrical properties of biological tissues allows it to detect abnormalities that would otherwise be angiographically invisible. Accordingly, many research groups are now focused on the commercialization of EIT sensors, prioritizing their clinical significance and ease of access. In 1999, the Food and Drug Administration (FDA) approved the first EIT device for its application in the detection of breast cancer (Adler and Holder, 2022). Since then, more than three companies have created new EIT systems and successfully placed them on the market for clinical use.

5.3 Intravascular sensors

Another biomedical application of EIS technology is in the field of intravascular sensors, which was first used in animal models to test for the buildup of plaque (Süselbeck et al., 2005). Because intravascular sensors are an *in vivo* application of impedance-based sensors, biocompatibility must be heavily considered in order for it to be clinically translational. In this study, four electrodes were coated with platinum (Pt) and placed on a flexible polyimide substrate. Later on, a similar study fabricated a catheter with Au electrodes and parylene C substrate to be tested on New Zealand white rabbits with hyperlipidemia (Cao et al., 2014). This device was first tested on the aortic explants of these rabbits, followed by *in vivo* testing to demonstrate biocompatibility. Parylene C has been shown to be an effective alternate substrate material to polyimide, yielding similar results during *in vivo* biocompatibility tests (del Valle et al., 2015). It was concluded that the impedance of Au electrodes is most sensitive between 10 kHz and 300 kHz for biological applications (Cao et al., 2014).

To further improve the study of intravascular sensors, this study further incorporated IVUS, along with an EIS sensor to enhance quality of images (Ma et al., 2016). EIS can detect calcification, oxidized LDL, and foam cells, while IVUS can detect thin-cap fibroatheroma, calcification, and fibrous structure. By combining these two sensing technologies together, we can gather data which contain information on all five of the intravascular components. The studies performed *ex vivo* on New Zealand White Rabbits showed reliability and consistency with results gathered from histology segments of the vasculature.

Another way researchers are constantly improving EIS is by incorporating new nanomaterials in order to increase the specificity of their devices. Nanomaterials with higher effective surface area decrease the impedance of devices, therefore increasing their specificity. In one particular study, the incorporation of Pt-Black onto electrodes via electroporation increases the accuracy of two-point electrodes in EIS sensors (Abiri et al., 2022). The Pt-Black sensors were tested on Yucatan mini pigs *in vivo* after a 16 week long high fat diet with partial ligation of the right carotid arteries (**Figure 7E**). This sensor proves the capability of sensing the high lipid content in the vasculature of Yucatan mini pigs. **Figure 7F** shows a three-dimensional rendering of impedimetric data gathered from the Pt-Black electrodes used for this study.

6 Perspectives

The emergence of conductive nanomaterials has undoubtedly revolutionized the field of bioimpedance sensors. However, as we enter a post Moore's era, the future outlook of conducting nanomaterials for bioimpedance sensors remains unclear (Iwai, 2016). The ratio of the effective surface area to macroscopic surface area begins to approach a certain limit, hindering the ability of new materials to significantly improve the sensitivity of EIS. This effect is evidenced by a nominal or sometimes downward trend of new publications with the keyword "carbon nanotubes," "gold nanoparticles," or "nanomotors," according to data recorded between 2010 and 2018 (Arduini et al., 2020). Even currently trending nanomaterials, such as graphene derivatives, are not immune to the limiting repercussions of post Moore's era.

Despite the uncertainty of future research, many of the nanomaterials discussed in this review are still in their early stages of discovery. There remains a large sum of work to be done on the commercialization and mass-production of nanomaterial-coated EIS electrodes, particularly ensuring that all requirements set by the FDA are met. As previously discussed, several classes of nanomaterials can be further functionalized to improve biocompatibility and clinical translation. Going forward, it is essential to balance the promise of novel materials with the practicalities of scaling up production and ensuring safety for clinical trials.

Author contributions

JC, BA, KW, and SW contributed to the literature search and writing of this review. JC wrote the introduction and background sections. JC and BA wrote the biomedical application and perspectives sections. KW wrote the nanomaterials section. SW wrote the wearable and implantable bioelectronics section. JY compiled the figures. TKH supervised the project. All authors

contributed to manuscript revision, read, and approved the submitted version.

Funding

This project was supported by NIH R01HL111437 (TKH), R01HL118650 (TKH), and R01HL149808 (TKH).

Conflict of interest

The authors declare that the research was conducted in the absence of any commercial or financial relationships that could be construed as a potential conflict of interest.

Publisher's note

All claims expressed in this article are solely those of the authors and do not necessarily represent those of their affiliated organizations, or those of the publisher, the editors and the reviewers. Any product that may be evaluated in this article, or claim that may be made by its manufacturer, is not guaranteed or endorsed by the publisher.

References

Abiri, P., Luo, Y., Huang, Z.-Y., Cui, Q., Duarte-Vogel, S., Roustaei, M., et al. (2022). 3-dimensional electrical impedance spectroscopy for *in situ* endoluminal mapping of metabolically active plaques. *Sensors Actuators B Chem.* 354, 131152. doi:10.1016/j.snb.2021.131152

Adler, A., and Holder, D. (2022). *Devices, history and conferences*. Boca Raton, Florida: CRC Press.

Adler, A., and Lionheart, W. R. B. (2006). Uses and abuses of EIDORS: An extensible software base for EIT. *Physiol. Meas.* 27, S25–S42. doi:10.1088/0967-3334/27/5/S03

Arduini, F., Cinti, S., Scognamiglio, V., and Moscone, D. (2020). "13 - nanomaterial-based sensors," in *Handbook of nanomaterials in analytical chemistry*. Editor C. Mustansar Hussain (Amsterdam, Netherlands: Elsevier), 329–359. doi:10.1016/B978-0-12-816699-4.00013-X

Bachmann, M. C., Morais, C., Bugedo, G., Bruhn, A., Morales, A., Borges, J. B., et al. (2018). Electrical impedance tomography in acute respiratory distress syndrome. *Crit. Care* 22, 263. doi:10.1186/s13054-018-2195-6

Banerjee, A., Tai, Y., Myung, N. V., and Nam, J. (2022). Non-destructive characterization of bone mineral content by machine learning-assisted electrochemical impedance spectroscopy. *Front. Bioeng. Biotechnol.* 10, 961108. doi:10.3389/fbioe.2022.961108

Bogomolova, A., Komarova, E., Reber, K., Gerasimov, T., Yavuz, O., Bhatt, S., et al. (2009). Challenges of electrochemical impedance spectroscopy in protein biosensing. *Anal. Chem.* 81, 3944–3949. doi:10.1021/ac9002358

Bolotsky, A., Butler, D., Dong, C., Gerace, K., Glavin, N. R., Muratore, C., et al. (2019). Two-dimensional materials in biosensing and healthcare: From *in Vitro* diagnostics to optogenetics and beyond. *ACS Nano* 13, 9781–9810. doi:10.1021/acsnano.9b03632

Brazey, B., Haddab, Y., and Zemiti, N. (2022). Robust imaging using electrical impedance tomography: Review of current tools. *Proc. R. Soc. A Math. Phys. Eng. Sci.* 478, 20210713. doi:10.1098/rspa.2021.0713

Bredar, A. R. C., Chown, A. L., Burton, A. R., and Farnum, B. H. (2020). Electrochemical impedance spectroscopy of metal oxide electrodes for energy applications. *ACS Appl. Energy Mater.* 3, 66–98. doi:10.1021/acsaem.9b01965

Brown, M. A., Goel, A., and Abbas, Z. (2016). Effect of electrolyte concentration on the stern layer thickness at a charged interface. *Angew. Chem. Int. Ed.* 55, 3790–3794. doi:10.1002/anie.201512025

Brunt, E. M., Wong, V. W.-S., Nobili, V., Day, C. P., Sookoian, S., Maher, J. J., et al. (2015). Nonalcoholic fatty liver disease. *Nat. Rev. Dis. Prim.* 1, 15080. doi:10.1038/nrdp.2015.80

Cao, H., Yu, F., Zhao, Y., Scianmarello, N., Lee, J., Dai, W., et al. (2014). Stretchable electrochemical impedance sensors for intravascular detection of lipid-rich lesions in New Zealand white rabbits. *Biosens. Bioelectron.* 54, 610–616. doi:10.1016/j.bios.2013.11.059

Carminati, M., Ferrari, G., Bianchi, D., and Sampietro, M. (2022). *Impedance spectroscopy for biosensing: Circuits and applications*. New York, NY: Springer New York, 87–110. doi:10.1007/978-1-4614-3447-4_30

Castro, A. C. H., Bezerra, I. R. S., Pascon, A. M., da Silva, G. H., Philot, E. A., de Oliveira, V. L., et al. (2022). Modular label-free electrochemical biosensor loading nature-inspired peptide toward the widespread use of COVID-19 antibody tests. *ACS Nano* 16, 14239–14253. doi:10.1021/acsnano.2c04364

Chakraborty, A., Tibarewala, D. N., and Barui, A. (2019). "5 - impedance-based biosensors," in *Bioelectronics and medical devices*. Editors K. Pal, H.-B. Kraatz, A. Khasnobish, S. Bag, I. Banerjee, and U. Kuruganti (Sawston, United Kingdom: Woodhead Publishing), 97–122. Woodhead Publishing Series in Electronic and Optical Materials. doi:10.1016/B978-0-08-102420-1.00005-4

Chang, C.-C., Huang, Z.-Y., Shih, S.-F., Luo, Y., Ko, A., Cui, Q., et al. (2021). Electrical impedance tomography for non-invasive identification of fatty liver infiltrate in overweight individuals. *Sci. Rep.* 11, 19859. doi:10.1038/s41598-021-99132-z

Chen, C., Wang, X., Li, M., Fan, Y., and Sun, R. (2018). Humidity sensor based on reduced graphene oxide/lignosulfonate composite thin-film. *Sensors Actuators B Chem.* 255, 1569–1576. doi:10.1016/j.snb.2017.08.168

Chen, T., Li, M., and Liu, J. (2018). π–π stacking interaction: A nondestructive and facile means in material engineering for bioapplications. *Cryst. Growth & Des.* 18, 2765–2783. doi:10.1021/acs.cgd.7b01503

Chen, Y., Lu, S., Zhang, S., Li, Y., Qu, Z., Chen, Y., et al. (2017). Skin-like biosensor system via electrochemical channels for noninvasive blood glucose monitoring. *Sci. Adv.* 3, e1701629. doi:10.1126/sciadv.1701629

Cho, S. (2008). "Electrical impedance spectroscopy for intravascular diagnosis of atherosclerosis," in *EKC2008 proceedings of the EU-korea conference on science and technology*. Editor S.-D. Yoo (Berlin, Heidelberg: Springer), 395–403.

Choi, C., Lee, Y., Cho, K. W., Koo, J. H., and Kim, D.-H. (2019). Wearable and implantable soft bioelectronics using two-dimensional materials. *Accounts Chem. Res.* 52, 73–81. doi:10.1021/acs.accounts.8b00491

Choi, S., Han, S. I., Jung, D., Hwang, H. J., Lim, C., Bae, S., et al. (2018). Highly conductive, stretchable and biocompatible Ag–Au core–sheath nanowire composite for wearable and implantable bioelectronics. *Nat. Nanotechnol.* 13, 1048–1056. doi:10.1038/s41565-018-0226-8

Davis, J. A., James, R. O., and Leckie, J. O. (1978). Surface ionization and complexation at the oxide/water interface: I. Computation of electrical double layer properties in simple electrolytes. *J. Colloid Interface Sci.* 63, 480–499. doi:10.1016/S0021-9797(78)80009-5

Dean, D., Ramanathan, T., Machado, D., and Sundararajan, R. (2008). Electrical impedance spectroscopy study of biological tissues. *J. Electrost.* 66, 165–177. doi:10.1016/j.elstat.2007.11.005

del Valle, J., de la Oliva, N., Müller, M., Stieglitz, T., and Navarro, X. (2015). "Biocompatibility evaluation of parylene c and polyimide as substrates for peripheral nerve interfaces," in 2015 7th International IEEE/EMBS Conference on Neural Engineering (NER), Montpellier, France, 22-24 April 2015, 442–445. doi:10.1109/NER.2015.7146654

Dijk, G., Ruigrok, H. J., and O'Connor, R. P. (2020). Influence of pedot:pss coating thickness on the performance of stimulation electrodes. *Adv. Mater. Interfaces* 7, 2000675. doi:10.1002/admi.202000675

Fahmy Taha, M. H., Ashraf, H., and Caesarendra, W. (2020). A brief description of cyclic voltammetry transducer-based non-enzymatic glucose biosensor using synthesized graphene electrodes. *Appl. Syst. Innov.* 3, 32. doi:10.3390/asi3030032

Faia, P. M., Silva, R., Rasteiro, M. G., Garcia, F. A. P., Ferreira, A. R., Santos, M. J., et al. (2012). Imaging particulate two-phase flow in liquid suspensions with electric impedance tomography. *Part. Sci. Technol.* 30, 329–342. doi:10.1080/02726351.2011.575444

Franks, W., Schenker, I., Schmutz, P., and Hierlemann, A. (2005). Impedance characterization and modeling of electrodes for biomedical applications. *IEEE Trans. Biomed. Eng.* 52, 1295–1302. doi:10.1109/TBME.2005.847523

Gasiorowski, J., Menon, R., Hingerl, K., Dachev, M., and Sariciftci, N. S. (2013). Surface morphology, optical properties and conductivity changes of poly(3,4-ethylenedioxythiophene):poly(styrenesulfonate) by using additives. *Thin Solid Films* 536, 211–215. doi:10.1016/j.tsf.2013.03.124

Halter, R., Hartov, A., and Paulsen, K. (2008). Video rate electrical impedance tomography of vascular changes: Preclinical development. *Physiol. Meas.* 29, 349–364. doi:10.1088/0967-3334/29/3/006

Hantanasirisakul, K., and Gogotsi, Y. (2018). Electronic and optical properties of 2d transition metal carbides and nitrides (mxenes). *Adv. Mater.* 30, 1804779. doi:10.1002/adma.201804779

Henderson, R. P., and Webster, J. G. (1978). An impedance camera for spatially specific measurements of the thorax. *IEEE Trans. Biomed. Eng.* 25, 250–254. doi:10.1109/TBME.1978.326329

Hinderliter, B., Croll, S., Tallman, D., Su, Q., and Bierwagen, G. (2006). Interpretation of eis data from accelerated exposure of coated metals based on modeling of coating physical properties. *Electrochimica Acta* 51, 4505–4515. doi:10.1016/j.electacta.2005.12.047

Holm, S., Holm, T., and Martinsen, Ø. G. (2021). Simple circuit equivalents for the constant phase element. *PLOS ONE* 16, e0248786. doi:10.1371/journal.pone.0248786

Hondroulis, E., Zhang, Z., Chen, C., and Li, C.-Z. (2012). Impedance based nanotoxicity assessment of graphene nanomaterials at the cellular and tissue level. *Anal. Lett.* 45, 272–282. doi:10.1080/00032719.2011.633184

Hu, K., Lan, D., Li, X., and Zhang, S. (2008). Electrochemical dna biosensor based on nanoporous gold electrode and multifunctional encoded dna-au bio bar codes. *Anal. Chem.* 80, 9124–9130. doi:10.1021/ac8017197

Huang, X., Li, H., Li, J., Huang, L., Yao, K., Yiu, C. K., et al. (2022). Transient, implantable, ultrathin biofuel cells enabled by laser-induced graphene and gold nanoparticles composite. *Nano Lett.* 22, 3447–3456. doi:10.1021/acs.nanolett.2c00864

Iravani, S., and Varma, R. S. (2022). Mxene-based composites as nanozymes in biomedicine: A perspective. *Nano-Micro Lett.* 14, 213. doi:10.1007/s40820-022-00958-7

Iwai, H. (2016). "End of the scaling theory and moore's law," in 2016 16th International Workshop on Junction Technology (IWJT), Shanghai, China, 09-10 May 2016, 1–4. doi:10.1109/IWJT.2016.7486661

Jash, P., Parashar, R. K., Fontanesi, C., and Mondal, P. C. (2022). The importance of electrical impedance spectroscopy and equivalent circuit analysis on nanoscale molecular electronic devices. *Adv. Funct. Mater.* 32, 2109956. doi:10.1002/adfm.202109956

Kesler, V., Murmann, B., and Soh, H. T. (2020). Going beyond the debye length: Overcoming charge screening limitations in next-generation bioelectronic sensors. *ACS Nano* 14, 16194–16201. PMID: 33226776. doi:10.1021/acsnano.0c08622

Kim, K. S., Um, Y. M., Jang, J.-r., Choe, W.-S., and Yoo, P. J. (2013). Highly sensitive reduced graphene oxide impedance sensor harnessing π-stacking interaction mediated direct deposition of protein probes. *ACS Appl. Mater. Interfaces* 5, 3591–3598. doi:10.1021/am303238r

Koo, W.-T., Jang, J.-S., and Kim, I.-D. (2019). Metal-organic frameworks for chemiresistive sensors. *Chem* 5, 1938–1963. doi:10.1016/j.chempr.2019.04.013

Kuk, W.-J., and Wright, N. R. (2022). Bedside diagnosis of pulmonary embolism using electrical impedance tomography: A case report. *A A Pract.* 16, e01606. doi:10.1213/xaa.0000000000001606

Lai, C.-Y., Huang, W.-C., Weng, J.-H., Chen, L.-C., Chou, C.-F., and Wei, P.-K. (2020). Impedimetric aptasensing using a symmetric randles circuit model. *Electrochimica Acta* 337, 135750. doi:10.1016/j.electacta.2020.135750

Lee, B., Li, K., Yoon, H. S., Yoon, J., Mok, Y., Lee, Y., et al. (2016). Membrane of functionalized reduced graphene oxide nanoplates with angstrom-level channels. *Sci. Rep.* 6, 28052. doi:10.1038/srep28052

Lee, H., Song, C., Hong, Y. S., Kim, M., Cho, H. R., Kang, T., et al. (2017). Wearable/disposable sweat-based glucose monitoring device with multistage transdermal drug delivery module. *Sci. Adv.* 3, e1601314. doi:10.1126/sciadv.1601314

Li, N., Wang, Q., Shen, C., Wei, Z., Yu, H., Zhao, J., et al. (2020). Large-scale flexible and transparent electronics based on monolayer molybdenum disulfide field-effect transistors. *Nat. Electron.* 3, 711–717. doi:10.1038/s41928-020-00475-8

Li, Y., Wang, S., Zhang, J., Ma, X., Cao, S., Sun, Y., et al. (2022). A highly stretchable and permeable liquid metal micromesh conductor by physical deposition for epidermal electronics. *ACS Appl. Mater. Interfaces* 14, 13713–13721. doi:10.1021/acsami.1c25206

Lim, H. J., Saha, T., Tey, B. T., Tan, W. S., and Ooi, C. W. (2020). Quartz crystal microbalance-based biosensors as rapid diagnostic devices for infectious diseases. *Biosens. Bioelectron.* 168, 112513. doi:10.1016/j.bios.2020.112513

Lin, S., Xu, L., Chi Wang, A., and Wang, Z. L. (2020). Quantifying electron-transfer in liquid-solid contact electrification and the formation of electric double-layer. *Nat. Commun.* 11, 399. doi:10.1038/s41467-019-14278-9

Liu, J., Xu, Y., Liu, S., Yu, S., Yu, Z., and Low, S. S. (2022). Application and progress of chemometrics in voltammetric biosensing. *Biosensors* 12, 494. doi:10.3390/bios12070494

Liu, R., Jin, C., Song, F., and Liu, J. (2013). Nanoparticle-enhanced electrical impedance detection and its potential significance in image tomography. *Int. J. Nanomedicine* 8, 33–38. doi:10.2147/IJN.S37275

Lu, Y., Lyu, H., Richardson, A. G., Lucas, T. H., and Kuzum, D. (2016). Flexible neural electrode array based-on porous graphene for cortical microstimulation and sensing. *Sci. Rep.* 6, 33526. doi:10.1038/srep33526

Luo, Y., Abiri, P., Zhang, S., Chang, C.-C., Kaboodrangi, A. H., Li, R., et al. (2018). Non-invasive electrical impedance tomography for multi-scale detection of liver fat content. *Theranostics* 8, 1636–1647. doi:10.7150/thno.22233

Lv, J., Liu, Y., Qin, Y., Yin, Q., Chen, S., Cheng, Z., et al. (2021a). Constructing "rigid-and-soft" interlocking stereoscopic interphase structure of aramid fiber composites with high interfacial shear strength and toughness. *Compos. Part A Appl. Sci. Manuf.* 145, 106386. doi:10.1016/j.compositesa.2021.106386

Lv, J., Yin, J., Qin, Y., Dai, Y., Cheng, Z., Luo, L., et al. (2021b). Post-construction of weaving structure in aramid fiber towards improvements of its transverse properties. *Compos. Sci. Technol.* 208, 108780. doi:10.1016/j.compscitech.2021.108780

Lymperopoulos, G., Lymperopoulos, P., Alikari, V., Dafogianni, C., Zyga, S., and Margari, N. (2017). "Applications for electrical impedance tomography (EIT) and electrical properties of the human body," in *GeNeDis 2016*. Editor P. Vlamos (Cham: Springer International Publishing), 109–117. doi:10.1007/978-3-319-57348-9_9

Ma, J., Luo, Y., Packard, R. R., Ma, T., Ding, Y., Abiri, P., et al. (2016). Ultrasonic transducer-guided electrochemical impedance spectroscopy to assess lipid-laden plaques. *Sensors Actuators B Chem.* 235, 154–161. doi:10.1016/j.snb.2016.04.179

Ma, X., Zhang, M., Zhang, J., Wang, S., Cao, S., Li, Y., et al. (2022). Highly permeable and ultrastretchable liquid metal micromesh for skin-attachable electronics. *ACS Mater. Lett.* 4, 634–641. doi:10.1021/acsmaterialslett.1c00763

Magar, H. S., Hassan, R. Y. A., and Mulchandani, A. (2021). Electrochemical impedance spectroscopy (EIS): Principles, construction, and biosensing applications. *Sensors* 21, 6578. doi:10.3390/s21196578

Malhotra, B. D., and Ali, M. A. (2018). "Chapter 4 - biopolymeric nanostructures: Biosensors and bioimaging," in *Nanomaterials for biosensors*. Editors B. D. Malhotra, and M. A. Ali (Norwich, NY.: William Andrew Publishing), 127–144. Micro and Nano Technologies. doi:10.1016/B978-0-323-44923-6.00004-2

Mansouri, S., Alharbi, Y., Haddad, F., Chabcoub, S., Alshrouf, A., and Abd-Elghany, A. A. (2021). Electrical impedance tomography – recent applications and developments. *J. Electr. Bioimpedance* 12, 50–62. doi:10.2478/joeb-2021-0007

Mayer, M., Xiao, X., Yin, J., Chen, G., Xu, J., and Chen, J. (2022). Advances in bioinspired triboelectric nanogenerators. *Adv. Electron. Mater.* 8, 2200782. doi:10.1002/aelm.202200782

Merrill, D. R. (2010). *The electrochemistry of charge injection at the electrode/tissue interface*. New York, NY: Springer New York, 85–138. doi:10.1007/978-0-387-98120-8_4

Mirceski, V., Skrzypek, S., and Stojanov, L. (2018). Square-wave voltammetry. *ChemTexts* 4, 17. doi:10.1007/s40828-018-0073-0

Miyamoto, A., Lee, S., Cooray, N. F., Lee, S., Mori, M., Matsuhisa, N., et al. (2017). Inflammation-free, gas-permeable, lightweight, stretchable on-skin electronics with nanomeshes. *Nat. Nanotechnol.* 12, 907–913. doi:10.1038/nnano.2017.125

Moon, J., Jiang, H., and Lee, E.-C. (2021). Physical surface modification of carbon-nanotube/polydimethylsiloxane composite electrodes for high-sensitivity DNA detection. *Nanomaterials* 11, 2661. doi:10.3390/nano11102661

Moore, D. C., Jawaid, A., Busch, R., Brothers, M., Miesle, P., Miesle, A., et al. (2022). Ultrasensitive molecular sensors based on real-time impedance spectroscopy in solution-processed 2D materials. *Adv. Funct. Mater.* 32, 2106830. doi:10.1002/adfm.202106830

Naguib, M., Kurtoglu, M., Presser, V., Lu, J., Niu, J., Heon, M., et al. (2011). Two-dimensional nanocrystals produced by exfoliation of ti3alc2. *Adv. Mater.* 23, 4248–4253. doi:10.1002/adma.201102306

Nezakati, T., Seifalian, A., Tan, A., and Seifalian, A. M. (2018). Conductive polymers: Opportunities and challenges in biomedical applications. *Chem. Rev.* 118, 6766–6843. doi:10.1021/acs.chemrev.6b00275

Nissinen, A., Kaipio, J. P., Vauhkonen, M., and Kolehmainen, V. (2015). Contrast enhancement in eit imaging of the brain. *Physiol. Meas.* 37, 1–24. doi:10.1088/0967-3334/37/1/1

Ostovari, M., Riahi Alam, N., Zabihzadeh, M., Gharibvand, M. M., and Hoseini-Ghahfarokhi, M. (2018). The effect of gold nanoparticles on electrical impedance of tissue on low frequency ranges. *J. Biomed. Phys. Eng.* 8, 241–250.

Packard, R. R. S., Luo, Y., Abiri, P., Jen, N., Aksoy, O., Suh, W. M., et al. (2017). 3-d electrochemical impedance spectroscopy mapping of arteries to detect metabolically active but angiographically invisible atherosclerotic lesions. *Theranostics* 7, 2431–2442. doi:10.7150/thno.19184

Packard, R. R. S., Zhang, X., Luo, Y., Ma, T., Jen, N., Ma, J., et al. (2016). Two-point stretchable electrode array for endoluminal electrochemical impedance spectroscopy measurements of lipid-laden atherosclerotic plaques. *Ann. Biomed. Eng.* 44, 2695–2706. doi:10.1007/s10439-016-1559-9

Pan, L., Cai, P., Mei, L., Cheng, Y., Zeng, Y., Wang, M., et al. (2020). A compliant ionic adhesive electrode with ultralow bioelectronic impedance. *Adv. Mater.* 32, 2003723. doi:10.1002/adma.202003723

Pang, Y., Yang, Z., Yang, Y., and Ren, T.-L. (2020). Wearable electronics based on 2d materials for human physiological information detection. *Small* 16, 1901124. doi:10.1002/smll.201901124

Park, D.-W., Schendel, A. A., Mikael, S., Brodnick, S. K., Richner, T. J., Ness, J. P., et al. (2014). Graphene-based carbon-layered electrode array technology for neural imaging and optogenetic applications. *Nat. Commun.* 5, 5258. doi:10.1038/ncomms6258

Park, K., Yuk, H., Yang, M., Cho, J., Lee, H., and Kim, J. (2022). A biomimetic elastomeric robot skin using electrical impedance and acoustic tomography for tactile sensing. *Sci. Robotics* 7, eabm7187. doi:10.1126/scirobotics.abm7187

Qi, D., Liu, Z., Liu, Y., Jiang, Y., Leow, W. R., Pal, M., et al. (2017). Highly stretchable, compliant, polymeric microelectrode arrays for *in vivo* electrophysiological interfacing. *Adv. Mater.* 29, 1702800. doi:10.1002/adma.201702800

Qiu, Q., Chen, H., Wang, Y., and Ying, Y. (2019). Recent advances in the rational synthesis and sensing applications of metal-organic framework biocomposites. *Coord. Chem. Rev.* 387, 60–78. doi:10.1016/j.ccr.2019.02.009

Raptopoulou, C. P. (2021). Metal-organic frameworks: Synthetic methods and potential applications. *Materials* 14, 310. doi:10.3390/ma14020310

Ravagli, E., Mastitskaya, S., Thompson, N., Iacoviello, F., Shearing, P. R., Perkins, J., et al. (2020). Imaging fascicular organization of rat sciatic nerves with fast neural electrical impedance tomography. *Nat. Commun.* 11, 6241. doi:10.1038/s41467-020-20127-x

Rodriguez, M. C., Kawde, A.-N., and Wang, J. (2005). Aptamer biosensor for label-free impedance spectroscopy detection of proteins based on recognition-induced switching of the surface charge. *Chem. Commun.* 4267, 4267–4269. doi:10.1039/B506571B

Sakr, Y., Giovini, M., Leone, M., Pizzilli, G., Kortgen, A., Bauer, M., et al. (2020). Pulmonary embolism in patients with coronavirus disease-2019 (COVID-19) pneumonia: A narrative review. *Ann. Intensive Care* 10, 124. doi:10.1186/s13613-020-00741-0

Sella, N., Pettenuzzo, T., Zarantonello, F., Andreatta, G., De Cassai, A., Schiavolin, C., et al. (2021). Electrical impedance tomography: A compass for the safe route to optimal peep. *Respir. Med.* 187, 106555. doi:10.1016/j.rmed.2021.106555

Seo, Y., and Wang, Z. J. (2021). Measurement and evaluation of specific absorption rate and temperature elevation caused by an artificial hip joint during mri scanning. *Sci. Rep.* 11, 1134. doi:10.1038/s41598-020-80828-7

Shah, P., Narayanan, T. N., Li, C.-Z., and Alwarappan, S. (2015). Probing the biocompatibility of mos2 nanosheets by cytotoxicity assay and electrical impedance spectroscopy. *Nanotechnology* 26, 315102. doi:10.1088/0957-4484/26/31/315102

Shen, S., Xiao, X., Yin, J., Xiao, X., and Chen, J. (2022). Self-powered smart gloves based on triboelectric nanogenerators. *Small Methods* 6, 2200830. doi:10.1002/smtd.202200830

Siegel, J., Kvitek, O., Kolska, Z., Slepicka, P., and Svorcik, V. (2012). "Gold nanostructures prepared on solid surface," in *Metallurgy*. Editor Y. Pardhi (Rijeka: IntechOpen). chap. 3. doi:10.5772/51617

Skale, S., Doleček, V., and Slemnik, M. (2007). Substitution of the constant phase element by warburg impedance for protective coatings. *Corros. Sci.* 49, 1045–1055. doi:10.1016/j.corsci.2006.06.027

Song, D., Ye, G., Zhao, Y., Zhang, Y., Hou, X., and Liu, N. (2022). An all-in-one, bioderived, air-permeable, and sweat-stable mxene epidermal electrode for muscle theranostics. *ACS Nano* 16, 17168–17178. doi:10.1021/acsnano.2c07646

Song, Y., Mukasa, D., Zhang, H., and Gao, W. (2021). Self-powered wearable biosensors. *Accounts Mater. Res.* 2, 184–197. doi:10.1021/accountsmr.1c00002

Strong, M. E., Richards, J. R., Torres, M., Beck, C. M., and La Belle, J. T. (2021). Faradaic electrochemical impedance spectroscopy for enhanced analyte detection in diagnostics. *Biosens. Bioelectron.* 177, 112949. doi:10.1016/j.bios.2020.112949

Su, F., Zhang, S., Ji, H., Zhao, H., Tian, J.-Y., Liu, C.-S., et al. (2017). Two-dimensional zirconium-based metal–organic framework nanosheet composites embedded with au nanoclusters: A highly sensitive electrochemical aptasensor toward detecting cocaine. *ACS Sensors* 2, 998–1005. doi:10.1021/acssensors.7b00268

Suni, I. I. (2008). Impedance methods for electrochemical sensors using nanomaterials. *Electroanal. Based Nanomater.* 27, 604–611. doi:10.1016/j.trac.2008.03.012

Süselbeck, T., Thielecke, H., Weinschenk, I., Reininger-Mack, A., Stieglitz, T., Metz, J., et al. (2005). *In vivo* intravascular electric impedancespectroscopy using a new catheter withintegrated microelectrodes. *Basic Res. Cardiol.* 100, 28–34. doi:10.1007/s00395-004-0501-8

Tapson, V. F. (2008). Acute pulmonary embolism. *N. Engl. J. Med.* 358, 1037–1052. doi:10.1056/nejmra072753

Tarcan, R., Todor-Boer, O., Petrovai, I., Leordean, C., Astilean, S., and Botiz, I. (2020). Reduced graphene oxide today. *J. Mat. Chem. C* 8, 1198–1224. doi:10.1039/C9TC04916A

Tybrandt, K., Khodagholy, D., Dielacher, B., Stauffer, F., Renz, A. F., Buzsáki, G., et al. (2018). High-density stretchable electrode grids for chronic neural recording. *Adv. Mater.* 30, 1706520. doi:10.1002/adma.201706520

Tyler, J., Choi, S. W., and Tewari, M. (2020). Real-time, personalized medicine through wearable sensors and dynamic predictive modeling: A new paradigm for clinical medicine. *Curr. Opin. Syst. Biol.* 20, 17–25. doi:10.1016/j.coisb.2020.07.001

Ud-Din, S., Wilgus, T. A., and Bayat, A. (2020). Mast cells in skin scarring: A review of animal and human research. *Front. Immunol.* 11, 552205. doi:10.3389/fimmu.2020.552205

Wang, A., Jung, D., Lee, D., and Wang, H. (2021a). Impedance characterization and modeling of subcellular to micro-sized electrodes with varying materials and pedot:pss coating for bioelectrical interfaces. *ACS Appl. Electron. Mater.* 3, 5226–5239. doi:10.1021/acsaelm.1c00687

Wang, K., Wu, C., Wang, F., and Jiang, G. (2018a). Mof-derived CoP_x nanoparticles embedded in nitrogen-doped porous carbon polyhedrons for nanomolar sensing of p-nitrophenol. *ACS Appl. Nano Mater.* 1, 5843–5853. doi:10.1021/acsanm.8b01501

Wang, K., Wu, C., Wang, F., Jing, N., and Jiang, G. (2019). Co/Co_3O_4 nanoparticles coupled with hollow nanoporous carbon polyhedrons for the enhanced electrochemical sensing of acetaminophen. *ACS Sustain. Chem. Eng.* 7, 18582–18592. doi:10.1021/acssuschemeng.9b04813

Wang, K., Wu, C., Wang, F., Liao, M., and Jiang, G. (2020). Bimetallic nanoparticles decorated hollow nanoporous carbon framework as nanozyme biosensor for highly sensitive electrochemical sensing of uric acid. *Biosens. Bioelectron.* 150, 111869. doi:10.1016/j.bios.2019.111869

Wang, K., Wu, C., Wang, F., Liu, C., Yu, C., and Jiang, G. (2018b). *In-situ* insertion of carbon nanotubes into metal-organic frameworks-derived α-Fe_2O_3 polyhedrons for highly sensitive electrochemical detection of nitrite. *Electrochimica Acta* 285, 128–138. doi:10.1016/j.electacta.2018.07.228

Wang, M., Yang, Y., Min, J., Song, Y., Tu, J., Mukasa, D., et al. (2022). A wearable electrochemical biosensor for the monitoring of metabolites and nutrients. *Nat. Biomed. Eng.* 6, 1225–1235. doi:10.1038/s41551-022-00916-z

Wang, S., Nie, Y., Zhu, H., Xu, Y., Cao, S., Zhang, J., et al. (2022). Intrinsically stretchable electronics with ultrahigh deformability to monitor dynamically moving organs. *Sci. Adv.* 8, eabl5511. eabl5511. doi:10.1126/sciadv.abl5511

Wang, S., Zhu, X., Meng, Q., Zheng, P., Zhang, J., He, Z., et al. (2021). Gold interdigitated micro-immunosensor based on Mn-MOF-74 for the detection of listeria monocytogens. *Biosens. Bioelectron.* 183, 113186. doi:10.1016/j.bios.2021.113186

Wang, X., Zhao, H., and Cui, N. (2021). The role of electrical impedance tomography for management of high-risk pulmonary embolism in a postoperative patient. *Front. Med.* 8, 773471. doi:10.3389/fmed.2021.773471

Wang, Y.-M., Zhang, X., Liu, C., Wu, L., Zhang, J., Lei, T., et al. (2022). Remarkable improvement of mof-based triboelectric nanogenerators with strong electron-withdrawing groups. *Nano Energy* 107, 108149. doi:10.1016/j.nanoen.2022.108149

Wen, T., Wang, R., Sotero, A., and Li, Y. (2017). A portable impedance immunosensing system for rapid detection of salmonella typhimurium. *Sensors* 17, 1973. doi:10.3390/s17091973

Xiao, X., Yin, J., Chen, G., Shen, S., Nashalian, A., and Chen, J. (2022a). Bioinspired acoustic textiles with nanoscale vibrations for wearable biomonitoring. *Matter* 5, 1342–1345. doi:10.1016/j.matt.2022.03.014

Xiao, X., Yin, J., Shen, S., Che, Z., Wan, X., Wang, S., et al. (2022b). Advances in solid-state fiber batteries for wearable bioelectronics. *Curr. Opin. Solid State Mater. Sci.* 26, 101042. doi:10.1016/j.cossms.2022.101042

Xu, B., Pei, J., Feng, L., and Zhang, X.-D. (2021). Graphene and graphene-related materials as brain electrodes. *J. Mat. Chem. B* 9, 9485–9496. doi:10.1039/D1TB01795K

Xu, J., Fang, Y., and Chen, J. (2021). Wearable biosensors for non-invasive sweat diagnostics. *Biosensors* 11, 245. doi:10.3390/bios11080245

Xu, K., Ji, X., Chen, C., Wan, H., Miao, L., and Jiang, J. (2015). Electrochemical double layer near polar reduced graphene oxide electrode: Insights from molecular dynamic study. *Electrochimica Acta* 166, 142–149. doi:10.1016/j.electacta.2015.03.101

Yan, Z., Xu, D., Lin, Z., Wang, P., Cao, B., Ren, H., et al. (2022). Highly stretchable van der waals thin films for adaptable and breathable electronic membranes. *Science* 375, 852–859. doi:10.1126/science.abl8941

Yang, H., Xue, T., Li, F., Liu, W., and Song, Y. (2019). Graphene: Diversified flexible 2D material for wearable vital signs monitoring. *Adv. Mater. Technol.* 4, 1800574. doi:10.1002/admt.201800574

Yao, B., Wu, S., Wang, R., Yan, Y., Cardenas, A., Wu, D., et al. (2022). Hydrogel ionotronics with ultra-low impedance and high signal fidelity across broad frequency and temperature ranges. *Adv. Funct. Mater.* 32, 2109506. doi:10.1002/adfm.202109506

Yin, L., Cao, M., Kim, K. N., Lin, M., Moon, J.-M., Sempionatto, J. R., et al. (2022). A stretchable epidermal sweat sensing platform with an integrated printed battery and electrochromic display. *Nat. Electron.* 5, 694–705. doi:10.1038/s41928-022-00843-6

Yoshioka, Y., Higashisaka, K., and Tsutsumi, Y. (2016). *Biocompatibility of nanomaterials*. New York, NY: Springer New York, 185–199. doi:10.1007/978-1-4939-3121-7_9

Yu, F., Dai, X., Beebe, T., and Hsiai, T. (2011a). Electrochemical impedance spectroscopy to characterize inflammatory atherosclerotic plaques. *Biosens. Bioelectron.* 30, 165–173. doi:10.1016/j.bios.2011.09.007

Yu, F., Li, R., Ai, L., Edington, C., Yu, H., Barr, M., et al. (2011b). Electrochemical impedance spectroscopy to assess vascular oxidative stress. *Ann. Biomed. Eng.* 39, 287–296. doi:10.1007/s10439-010-0127-y

Yu, Y., Nassar, J., Xu, C., Min, J., Yang, Y., Dai, A., et al. (2020). Biofuel-powered soft electronic skin with multiplexed and wireless sensing for human-machine interfaces. *Sci. Robotics* 5, eaaz7946. doi:10.1126/scirobotics.aaz7946

Yuan, H., Cheng, G., You, L., Li, H., Zhu, H., Li, W., et al. (2015). Influence of metal–mos2 interface on mos2 transistor performance: Comparison of ag and ti contacts. *ACS Appl. Mater. Interfaces* 7, 1180–1187. doi:10.1021/am506921y

Yuk, H., Lu, B., Lin, S., Qu, K., Xu, J., Luo, J., et al. (2020). 3d printing of conducting polymers. *Nat. Commun.* 11, 1604. doi:10.1038/s41467-020-15316-7

Zhai, Q., Yap, L. W., Wang, R., Gong, S., Guo, Z., Liu, Y., et al. (2020). Vertically aligned gold nanowires as stretchable and wearable epidermal ion-selective electrode for noninvasive multiplexed sweat analysis. *Anal. Chem.* 92, 4647–4655. PMID: 32069026. doi:10.1021/acs.analchem.0c00274

Zhang, F., Jin, T., Hu, Q., and He, P. (2018). Distinguishing skin cancer cells and normal cells using electrical impedance spectroscopy. *J. Electroanal. Chem.* 823, 531–536. doi:10.1016/j.jelechem.2018.06.021

Zhang, X., Zhang, D., Chen, Y., Sun, X., and Ma, Y. (2012). Electrochemical reduction of graphene oxide films: Preparation, characterization and their electrochemical properties. *Chin. Sci. Bull.* 57, 3045–3050. doi:10.1007/s11434-012-5256-2

Zhao, H., Zhou, Y., Cao, S., Wang, Y., Zhang, J., Feng, S., et al. (2021). Ultrastretchable and washable conductive microtextiles by coassembly of silver nanowires and elastomeric microfibers for epidermal human–machine interfaces. *ACS Mater. Lett.* 3, 912–920. doi:10.1021/acsmaterialslett.1c00128

Zhao, S. R., Mondéjar-Parreño, G., Li, D., Shen, M., and Wu, J. C. (2022). Technical applications of microelectrode array and patch clamp recordings on human induced pluripotent stem Cell-Derived cardiomyocytes. *JoVE* 186, e64265. doi:10.3791/64265

Zhao, X., Nashalian, A., Ock, I. W., Popoli, S., Xu, J., Yin, J., et al. (2022). A soft magnetoelastic generator for wind-energy harvesting. *Adv. Mater.* 34, 2204238. doi:10.1002/adma.202204238

Zhu, H., Wang, S., Zhang, M., Li, T., Hu, G., and Kong, D. (2021). Fully solution processed liquid metal features as highly conductive and ultrastretchable conductors. *NPJ Flex. Electron.* 5, 25. doi:10.1038/s41528-021-00123-x

Zukiene, K., Monastyreckis, G., Kilikevicius, S., Procházka, M., Micusik, M., Omastová, M., et al. (2021). Wettability of mxene and its interfacial adhesion with epoxy resin. *Mater. Chem. Phys.* 257, 123820. doi:10.1016/j.matchemphys.2020.123820